Article

ITRAQ Based Proteomics Reveals the Potential Mechanism of Placental Injury Induced by Prenatal Stress

Yujie Li [1,†], Junlin Hou [2,†], Liping Yang [2,*], Tong Zhang [2], Yu Jiang [2], Zhixing Du [2], Huizi Ma [2], Gai Li [2], Jianghui Zhu [2] and Ping Chen [3]

[1] Department of Biochemistry, School of Medicine, Henan University of Chinese Medicine, Zhengzhou 450046, China; lyj_happy@hactcm.edu.cn

[2] Department of Integrated Traditional Chinese and Western Medicine, School of Traditional Medicine, Henan University of Chinese Medicine, Zhengzhou 450046, China; houjunlin2005@163.com (J.H.); zhangtong1600@126.com (T.Z.); bio_jiangyu@126.com (Y.J.); dzx19961212@163.com (Z.D.); zydmhz@126.com (H.M.); 15225103693@163.com (G.L.); 15038268764@163.com (J.Z.)

[3] Gynaecology and Obstetrics, College of First Clinical Medical, Henan University of Chinese Medicine, Zhengzhou 450003, China; pinging6768@126.com

* Correspondence: jc.ylping@hactcm.edu.cn; Tel.: +86-0371-65835119

[†] These authors contributed equally to this work.

Abstract: Maternal stress experienced during prenatal development is recognized as a significant risk factor for neurodevelopmental and neuropsychiatric disorders across the offspring's lifespan. The placental barrier serves a crucial function in safeguarding the fetus from detrimental exposures during gestation. However, previous investigations have not yet comprehensively elucidated the extensive connections between prenatal stress and the expression of placental proteins. In this study, we used iTRAQ-based quantitative proteomics to elucidate the placental adaptive mechanisms of pregnant rats in response to fear-induced stress. Our results showed that during pregnancy, exposure to fear-induced stress led to a pathological hypercoagulable state in the mother's body. Placental circulation was also disrupted, significantly reducing placental efficiency and blood oxygen saturation in newborn rats. Proteomic analyses showed that most of the DEPs were annotated to the PI3K-Akt and ECM-receptor interaction signaling pathway. In addition, the expressions of CDC37, HSP90β, AKT, p-AKT and p-mTOR were down-regulated significantly in the placenta. Our results demonstrated that prenatal fear-induced stress led to inhibition of the cellular signal transduction of placental PI3K/AKT/mTOR, which affected biological processes such as rRNA processing, translation, protein folding, protein stability, and oxygen transport in the placenta. These abnormalities in biological functions could potentially damage the barrier function of the placenta and thereby result in abnormal development in the offspring.

Keywords: prenatal stress; placental damage; proteomics analyses; PI3K/AKT/mTOR pathway

1. Introduction

Prenatal exposure to maternal stress is a well-established risk factor for neurodevelopmental and neuropsychiatric disorders across the lifespan of offspring. Prenatal adverse experience alters the maternal biological environment, thus directly or indirectly affecting fetal development [1,2]. Studies have shown that prenatal stress impairs the growth and development of offspring. This includes the development of the nervous system, neurocognitive functions, the immune system, the autonomic nervous system, and the hypothalamo-pituitary-adrenal (HPA)-axis [3,4]. The mechanisms of those disorders are assumed to be associated with abnormal expressions of placental receptors and enzymes, which can directly disrupt placental function, promoting alterations in the epigenetic programming of the fetus [1,5]. The placental barrier is instrumental in safeguarding the fetus against deleterious environmental exposures throughout gestation. Nonetheless, maternal

chronic psychological stress can compromise this protective barrier, thereby elevating the likelihood of unfavorable developmental and health consequences [6]. The underlying molecular pathways that mediate these correlations remain poorly elucidated. Epigenetic modifications, including DNA methylation and RNA methylation, are postulated to serve as a molecular conduit connecting prenatal stress, placental barrier dysfunction, and subsequent adverse developmental and health outcomes [6]. Our prior investigative endeavors have elucidated that maternal stress induced by fear during gestation elevates the total methylation content within the placental tissue of pregnant rats. Notably, the m6A methylation modifications were predominantly localized within the coding sequences and the 3′ untranslated regions [7]. However, the implications of such epigenetic modifications on gene transcriptional activity are yet to be fully understood. Hence, the aim of the present study is to delineate the putative biological linkages between prenatal stress and placental pathological alterations through an integrative proteomic analysis. This could provide critical insights into the molecular underpinnings connecting prenatal stress, placental barrier dysfunction, and the subsequent adverse developmental and health consequences.

Our previous research has demonstrated that prenatal fear stress can precipitate depressive disorders in pregnant rats, which was found to be associated with behavioral anomalies and developmental delays in their progeny [2]. In the present study, we prepared a prenatal fear stress model (FSM) by observing and listening to the tragedy of electrically stimulated male rats according to the method described in our previous studies. Furthermore, to ascertain the model's scientific validity and replicability, we assessed the stress response of the pregnant rats through behavioral indices and the activation state of the hypothalamic-pituitary-adrenal (HPA) axis. Concurrently, we meticulously monitored the growth and developmental trajectory of the offspring, along with their behavioral manifestations, to maintain experimental accuracy. In addition, an unbiased proteomic profiling was achieved utilizing isobaric tags for relative and absolute quantification (iTRAQ). Subsequent to data acquisition, the STRING database and Cytoscape software were instrumental in constructing protein–protein interaction networks. Moreover, Gene Ontology (GO) analyses were conducted to delineate the principal functions of the differentially expressed proteins (DEPs), while the Kyoto Encyclopedia of Genes and Genomes (KEGG) facilitated the identification of prominent pathways associated with these DEPs. Validation of the findings was accomplished through western blotting and a battery of other biochemical analyses. These results might contribute to clarifying the complex molecular mechanisms of placental dysfunction due to prenatal stress and its adverse effects on offspring development. They could potentially inform the creation of diagnostic and preventive strategies for disorders related to prenatal psychological stress.

2. Results

2.1. Behavioral Assessment of Pregnant Rats

Following a 20-day exposure to fear-induced psychological stress, pregnant rats displayed marked behavioral aberrations. The sucrose consumption of FSM rats decreased significantly, the immobility time of TST increased significantly compared with that of NC rats ($p < 0.05$ or $p < 0.01$) (Figure 1A). In addition, regarding the OFT results, the frequency of ambulation and rearing decreased significantly ($p < 0.01$) (Figure 1B). These results suggest that the exploratory behavior of rats in the FSM group was reduced, along with an increase in anhedonia and anxiety-like behaviors. Furthermore, the serum ACTH and CORT concentrations of rats in FSM group were significantly elevated compared to those of NC rats ($p < 0.01$) (Figure 1C). These results suggested that fear-induced psychological stress led to high levels of stress hormones and caused behavior deficits in pregnant rats.
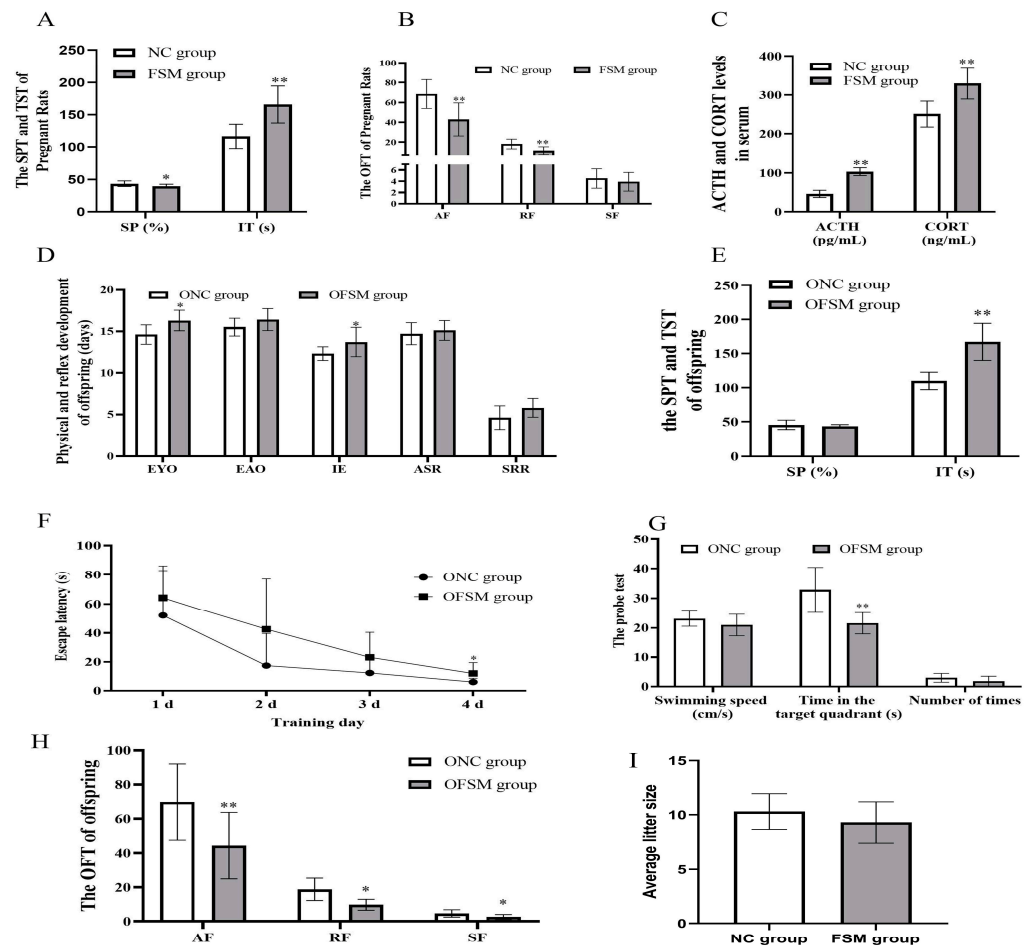
Figure 1. Behavioral assessment of pregnant rats and their pups. The results of (**A**) the Sucrose Preference Test and the immobility time of pregnant rats are presented. (**B**) The results of Open-Field Test of pregnant rats. (**C**) The concentrations of serum stress hormones in pregnant rats. (**D**) The physical and reflex development of offspring. (**E**) The sucrose consumption and the immobility times in the Tail suspension test of pups. (**F**) The escape latency during the 4 training days in the MWM and (**G**) the swimming speeds, the retention time that rats spent in the target quadrant, and the number of times that the pups crossed the original platform during the probe test in the MWM. (**H**) The frequency of ambulation, rearing, and self-grooming in the open field-tests of the pups. (**I**) The result of the average litter size of pregnant rats. NC group, normal control group; FSM group, fear stress model group; SP, Sucrose Preference; IT, immobility time; AF, Ambulation frequency: number of floor units entered with all four feet; RF, Rearing frequency, number of instances of standing on the hindlimbs without touching the wall; SF, Self-grooming frequency: number of self-grooming actions performed; ACTH, Adrenocorticotropic hormone; CORT, Corticosterone; OFSM, offspring from the FSM group; ONC, offspring from the normal control group; EYO, eye opening; EAO, ear opening; IE, incisor eruption; ASR, auditory startle reflex; SRR, surface righting reflex; MWM, Morris water maze. Values are expressed as means ± standard deviations.* $p < 0.05$, ** $p < 0.01$ versus NC group or ONC group.

2.2. Neurobehavioral and Developmental Milestones of the Pups

The results of the physical and neurobehavioral development of the pups are shown in Figure 1. No significant difference was observed in the average litter size between the two groups of pregnant rats ($p > 0.05$). The offspring from the FSM group (OFSM) demonstrated a pronounced extension in the duration of eye opening and incisor eruption when compared to ($p < 0.05$) those offspring from the NC group (ONC). While the ear opening, auditory startle reflex, and surface righting reflex of OFSM pups tended to be delayed in comparison to the ONC group, these differences did not reach statistical

significance ($p > 0.05$) (Figure 1D). These observations suggest that maternal fear stress during gestation may impede the physical and reflexive development of the offspring.

Behavioral assessments, encompassing the SPT, TST, OFT, and MWM Test, were conducted from PND 21–27 to gauge pup anxiety levels, as well as their learning and memory capabilities. There was no significant difference in sucrose consumption between the two offspring groups ($p > 0.05$). However, OFSM rats displayed a significant increase in immobility time relative to ONC rats ($p < 0.01$) (Figure 1E). In the OFT, a significant reduction was observed in the frequency of ambulation, rearing, and self-grooming behaviors in the OFSM rats ($p < 0.05$ or $p < 0.01$) (Figure 1H). Furthermore, a statistical analysis via Repeated-measures ANOVA revealed a significant impact of training duration on the rats' escape latency (F = 21.531, $p < 0.01$) (Figure 1F). Notably, both the ONC and OFSM groups exhibited learning progression, characterized by a continuous decrease in escape latency. However, the OFSM rats required a longer duration to reach the platform compared to the ONC rats (F = 4.694, $p < 0.05$). During the probe trial of the MWM, the OFSM rats demonstrated a significantly reduced retention time in the target quadrant compared to the ONC rats ($p < 0.01$). Despite this, no significant discrepancies were detected between the two groups in terms of swimming speed and frequency in crossing the original platform (Figure 1G). In addition, we analyzed the impact of sex on behavioral assessment results through Two-Way ANOVA. We discovered that there was a significant interaction between sex and rearing results, but no significant interaction with other behavioral results. These findings imply that maternal exposure to fear stress during gestation may augment anxiety- and depression-related behaviors, while also compromising the spatial learning and memory capabilities of the offspring.

2.3. The Impact of Maternal Psychological Stress on Placental Functionality and Oxygen Transfer

To evaluate placental efficiency, the weights of both the fetus and placenta were meticulously recorded. Oxygen saturation levels in the blood of both pregnant and neonatal rats were measured to ascertain the placental gas exchange capabilities. As shown in Figure 2A–D, exposure to fear stress during pregnancy significantly diminished fetal and placental weights, as well as the efficiency of the placenta, when contrasted with the non-stressed control group ($p < 0.01$). Moreover, the blood oxygen saturation in the FSM group was markedly lower compared to that of the control rats (Figure 2E). Additionally, the mean corpuscular volume (MCV) witnessed a pronounced reduction ($p < 0.01$) (Table 1), whereas there was a significant increase in platelet count and mean platelet volume within the FSM group. Furthermore, compared with NC rats, the APTT, TT, and the ATIII activation of FSM rats were significantly decreased ($p < 0.01$ or $p < 0.05$) (Figure 2G,H). These results suggested that maternal fear stress during gestation may elicit a hypercoagulable state, which potentially disrupts placental circulation and results in abnormalities in embryonic development.

Table 1. The complete blood cell counts (CBC) of pregnant rats were determined.

Index	NC Group	FSM Group
White blood cells ($\times 10^9$/L)	7.20 ± 2.92	3.48 ± 1.45 *
Lymphocyte ($\times 10^9$/L)	3.87 ± 1.02	2.12 ± 0.79 **
Monocyte ($\times 10^9$/L)	0.22 ± 0.12	0.17 ± 0.10
Neutrophil ($\times 10^9$/L)	3.12 ± 1.82	1.20 ± 0.59 *
Percentage of lymphocytes (%)	55.70 ± 7.86	62.23 ± 6.54
Percentage of monocytes (%)	3.42 ± 0.45	4.55 ± 1.22
Percentage of neutrophils (%)	40.88 ± 7.67	33.22 ± 5.49
Red blood cell ($\times 10^{12}$/L)	5.48 ± 0.27	5.70 ± 0.77
Hemoglobin (g/L)	107.00 ± 5.51	111.00 ± 13.67
Hematocrit (%)	33.33 ± 1.84	32.22 ± 3.62
Mean corpuscular volume (fL)	60.97 ± 1.44	56.80 ± 2.27 **

Table 1. *Cont.*

Index	NC Group	FSM Group
Mean corpuscular hemoglobin (pg)	19.50 ± 0.44	19.47 ± 0.46
Red cell distribution width (%)	12.32 ± 0.71	13.08 ± 1.41
Platelet ($\times 10^9$/L)	940.50 ± 128.04	1421.00 ± 275.97 **
Mean platelet volume (fL)	5.93 ± 0.24	8.07 ± 0.68 **

Note: * $p < 0.05$, ** $p < 0.01$ versus normal group.
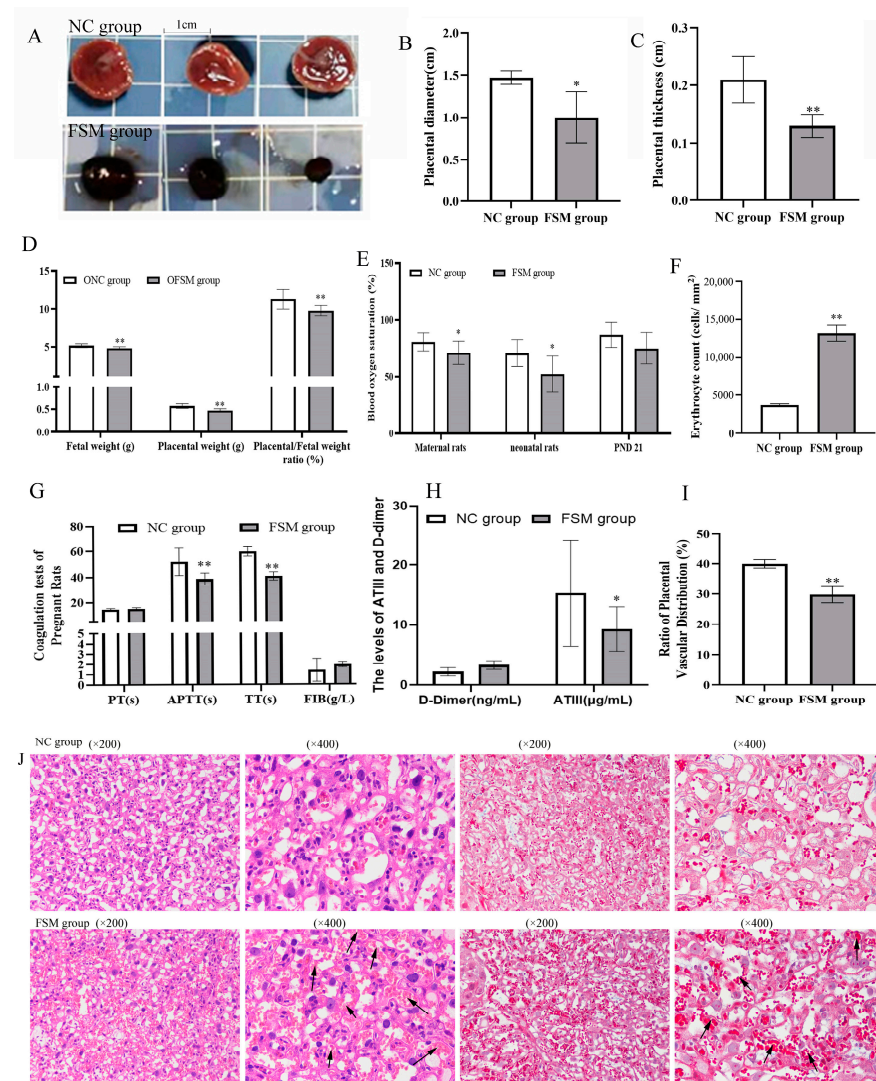
Figure 2. Effects of prenatal fear stress on placental efficiency, coagulatory biomarkers, and placental histopathology in pregnant rats. (**A**) the morphological features of placental tissues; (**B**) the diameters and (**C**) the thicknesses of placentas; (**D**) the weights of the fetus and placentas, and the placental efficiency; (**E**) the blood oxygen saturations of pregnant rats and their pups; (**F**) quantification of red blood cells in placental blood vessels using imageJ; (**G,H**) the coagulatory biomarkers of pregnant rats using the detection kits; (**I**) Quantitative analysis of the vascular network distribution in placental tissue using imageJ; (**J**) the H&E staining and Masson staining of the placentas were performed to evaluate the pathological changes of the placenta. The arrow indicates the presence of red blood cells within the blood vessels. NC group, normal control group; FSM group, fear stress model group; OFSM, offspring from the FSM group; ONC, offspring from the normal control group; PND 21, postnatal days of 21, PT, prothrombin time; APTT, activated partial thromboplastin time; TT, thrombin time; FIB, fibrinogen; ATIII, antithrombin III. Values are expressed as means $\pm$ standard deviations.* $p < 0.05$, ** $p < 0.01$ versus NC group or ONC group.

2.4. Effects of Prenatal Fear Stress on Placental Histomorphology in Rats

In the initial assessment, the gross morphological characteristics of placental tissue were examined. We noted that the NC group exhibited a lighter, cherry-red hue, in contrast to the FSM group, which demonstrated a more intense, purplish-red hue (Figure 2A). Furthermore, a marked decrease in both the diameter and the thickness of the placenta was noted in the FSM group when compared with the NC group (Figure 2B,C). Histological evaluations, including H&E staining and Masson staining, were conducted to evaluate the placental histopathological changes (Figure 2J). Our analysis revealed a diminished vascular network within the placentas of the FSM group (Figure 2I), accompanied by an increased number of red blood cells in the vascular channels observed under the microscope (Figure 2F). Those results might be related to the pathological hypercoagulable state of pregnant rats.

2.5. iTRAQ-Based Proteomic Analyses

The placenta plays an important role in gas exchange and nutrient transport between mother and fetus. Maternal psychological stress has the potential to perturb these interactions, subsequently impacting the somatic and neural development of the fetus [8]. To delineate the influence of maternal psychological stress on placental functionality, we conducted a proteomic study of placental proteins using iTRAQ coupled with LC-MS/MS techniques. In doing so, we identified 1753 proteins from 16,019 distinct peptides derived from 339,465 spectra with a high confidence ($\geq$95% confidence) and unique peptide matches $\geq$ 2. After excluding uncharacterized proteins and duplicate values caused by different peptide segments of the same protein, a total of 1730 proteins were identified. Using fold changes > 1.2 or <0.83 with *p*-value < 0.05 as a cutoff, 287 DEPs were identified between the two groups, including 145 upregulated proteins (Appendix A Table A1) and 142 downregulated proteins (Appendix A Table A2). The top 10 up- and down-regulated proteins in the placenta are shown in Table 2. Figure 3A depicts a quantitative volcanic map of differentially expressed proteins.

Table 2. Top 10 up- and down-regulated proteins in the placenta were show.

Gene Names	Protein Names	Fold Change	*p*-Value
Alb	Serum albumin	3.344481605	0.00107535
C4bpa	C4b-binding protein alpha chain	2.100840336	0.028742183
Plp2	Proteolipid protein 2	1.976284585	0.00518908
Slc40a1	Protein LOC100911874	1.923076923	0.004230614
Prl8a7	Prolactin-8A7	1.890359168	7.2348×10^{-6}
Slc7a5	Large neutral amino acids transporter small subunit 1	1.872659176	4.26129×10^{-10}
Fbn1	Fibrillin 1	1.824817518	0.035886107
Aqp1	Aquaporin-1	1.814882033	0.000190706
Vtn	Protein Vtn	1.76366843	0.000118123
Igh-1a	Ig gamma-2B chain C region	1.751313485	1.1581×10^{-19}
Rplp1	60S acidic ribosomal protein P1	0.619195046	0.000108538
Rps17	40S ribosomal protein S17	0.616522811	1.57927×10^{-12}
Rps25	40S ribosomal protein S25	0.61462815	2.51193×10^{-6}
Eif3e	Eukaryotic translation initiation factor 3 subunit E	0.612369871	0.010033231
Taldo1	Transaldolase	0.609756098	0.008266795
Hba2	Protein Hba2	0.463606861	5.45252×10^{-7}
Hbg1	Beta-globin chain (Fragment)	0.43554007	7.10019×10^{-6}
Hbz	Protein Hbz	0.410677618	4.77399×10^{-16}
Hba1	Hemoglobin subunit alpha-1/2	0.399361022	3.2938×10^{-15}

Figure 3. The volcano map of the identified proteins and GO classification of DEPs were shown. (**A**) The volcano map of the identified proteins was plotted based on its logarithmic fold change and *p*-value. *x*-axis represents the log2-fold change of protein expressions in FSM group compared to the NC group; The *y*-axis corresponds to the *p*-value of this fold change. Red dots: significant difference proteins; blue dots: proteins with fold changes > 0.83 or <1.2, and *p*-value < 0.05; grey and green dots: proteins with no significant difference in expression. (**B**–**D**) the GO classification of DEPs; (**B**) distributions of the DEPs for cellular components; (**C**) distributions of the DEPs for molecular functions; (**D**) distributions of the DEPs for biological processes. Only the top 20 Gene Ontology (GO) terms with significant differences (*p*-value < 0.05) are shown.

2.6. Protein–Protein Interaction (PPI) Network Construction and Hub Genes Extraction

The PPI network of these DEPs was performed by STRING software (STRING Database Version: 12.0), as presented in Figure 4. There were 170 nodes and 575 edges in the network. It consisted of 1 major network and 12 minor networks (Figure 4A). Utilizing the cytoHubba plug-in of Cytoscape software, hub genes were extracted from the PPI network (Figure 4B). A total of 39 hub genes were identified using eight different algorithms, encompassing 21 ribosomal proteins (involved in the translation process) and 18 additional proteins. These hub genes are predominantly involved in transcriptional regulation (Snrpd3), translation (21 ribosomal proteins, Eef2, and Eef1a1), protein folding and refolding (Hsp90ab1, Hspa1a, Tcp1, Cct5), and coagulation (C4bpa, Fgg, Serpine1) [9–12] during the critical phase of placental development.

Figure 4. PPI network construction and hub genes extraction of DEPs. (**A**) The PPI network of the DEPs is shown. Network nodes represent proteins; edges represent protein–protein associations. Network analysis was set at high confidence (STRING score = 0.4) and high FDR stringency (0.01). Red indicates significantly increased; green indicates significantly decreased; width represents the degree of the interactions. (**B**) The top 10 hub genes were extracted with cytoHubba plug-in of Cytoscape software, and the eight algorithms are shown. Network nodes represent proteins; edges represent protein–protein associations. Color represents the score. MCC, Matthews Correlation Coefficient; DMNC, Neighborhood Component Centrality; MNC, Maximum Neighbor Connectivity; EPC, Edge Percolated Component.

2.7. GO and KEGG Enrichment Analyses of DEPs

In pursuit of elucidating the impact of maternal psychological stress on placental functionality, GO annotation (Figure 3B–D) and KEGG pathway enrichment (Figure 5A) were conducted on the DEPs. The results indicated that fear stress during pregnancy significantly affects a diverse array of placental biological processes, encompassing blood coagulation, fibrin clot formation, Fibrinolysis, negative regulation of endopeptidase activity, rRNA processing, protein folding, protein stabilization, translation, oxygen transport, and other biological processes. The molecular function enrichment of DEPs was predominantly concentrated in protein binding, RNA binding, and structural constituent of ribosome and oxygen binding. According to the GO cellular component enrichment, the DEPs were predominantly situated within the cytosolic ribosome, basement membrane and cytoplasm. Pathway enrichment analysis highlighted the ECM-receptor interaction and the PI3K-Akt signaling pathway as the primary pathways associated with the DEPs.
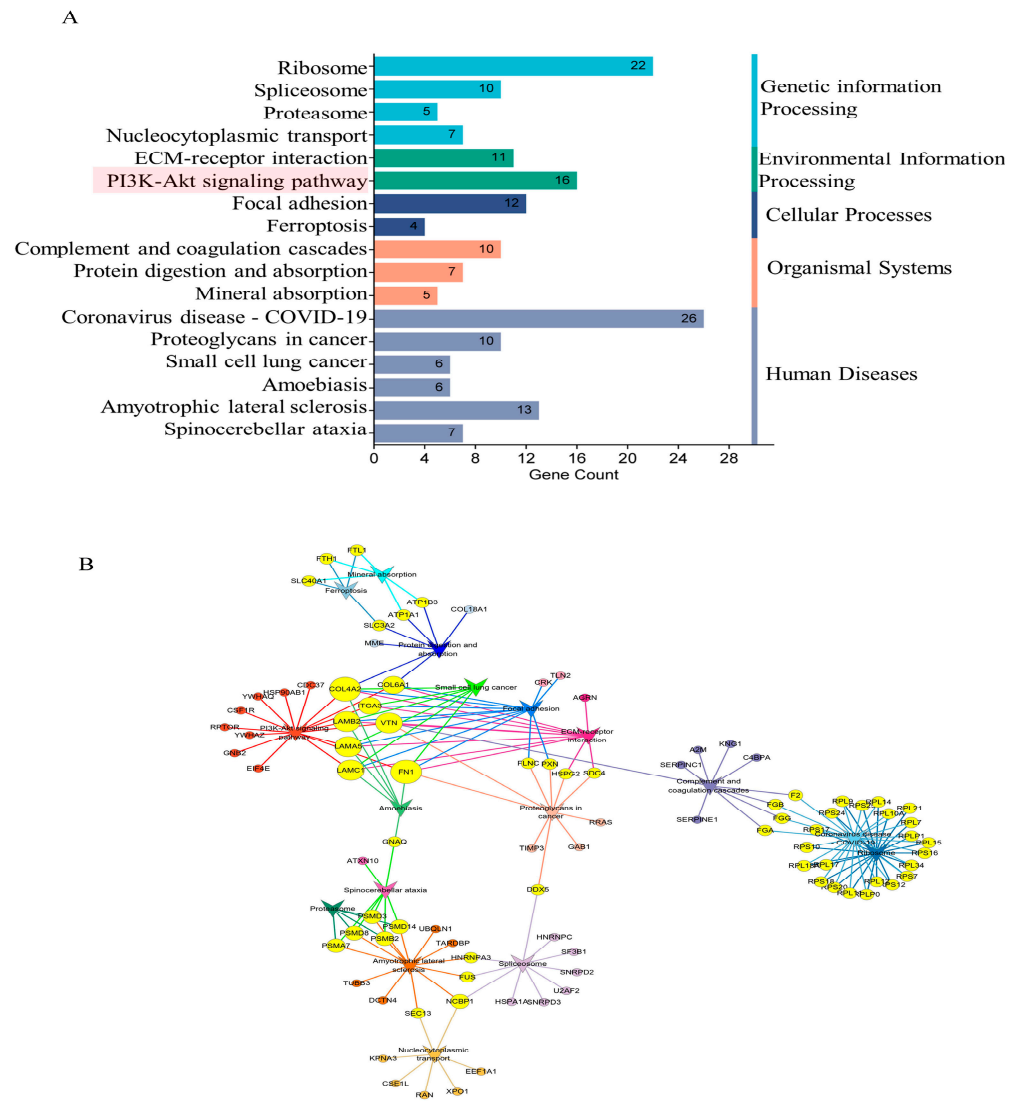
Figure 5. The results of KEGG enrichment of DEPs. (**A**) The significantly enriched pathways (*p*-value < 0.05). (**B**) The significant interactions of the pathways (*p*-value < 0.05). Circle-nodes represent DEPs. Arrow-shaped nodes represent the pathways. Edges represent connections between the nodes. Node color represents the pathways to which they belong. Yellow coloring represents the multiple pathways to which the proteins belong.

To delineate the precise contributions of ECM-receptor interaction and PI3K-Akt signaling pathway in the context of placental damage induced by fear stress, Cytoscape software was utilized to construct a comprehensive correlation network integrating the insights from pathway enrichment with the identified differential proteins (Figure 5B). The analysis suggested that the PI3K-Akt signaling pathway intersects with several pathways, including protein digestion and absorption, small cell lung cancer, focal adhesion, ECM-receptor interaction, proteoglycans in cancer and amoebiasis pathways. The results indicate that maternal psychological stress has the potential to perturb the PI3K-Akt signaling pathway, compromising the placenta's normal physiological functions, thereby impacting fetal physiological and neural development.

2.8. The Impact of Maternal Stress on Placental PI3K/AKT/mTOR Pathway Signaling

As shown in Figure 6, to explore the potential mechanisms of placental injury induced by fear stress, we conducted an analysis of placental protein expression, focusing on PI3K, p-PI3K AKT, p-AKT, mTOR, and p-mTOR expression. Compared with the NC

group, the expressions of PI3K and mTOR proteins were without significant changes ($p > 0.05$). However, the expressions of AKT, p-AKT, and p-mTOR decreased significantly. Therefore, fear stress may affect placental development via inhibiting cell signaling of PI3K/AKT/mTOR, without influencing the expressions of PI3K and mTOR.
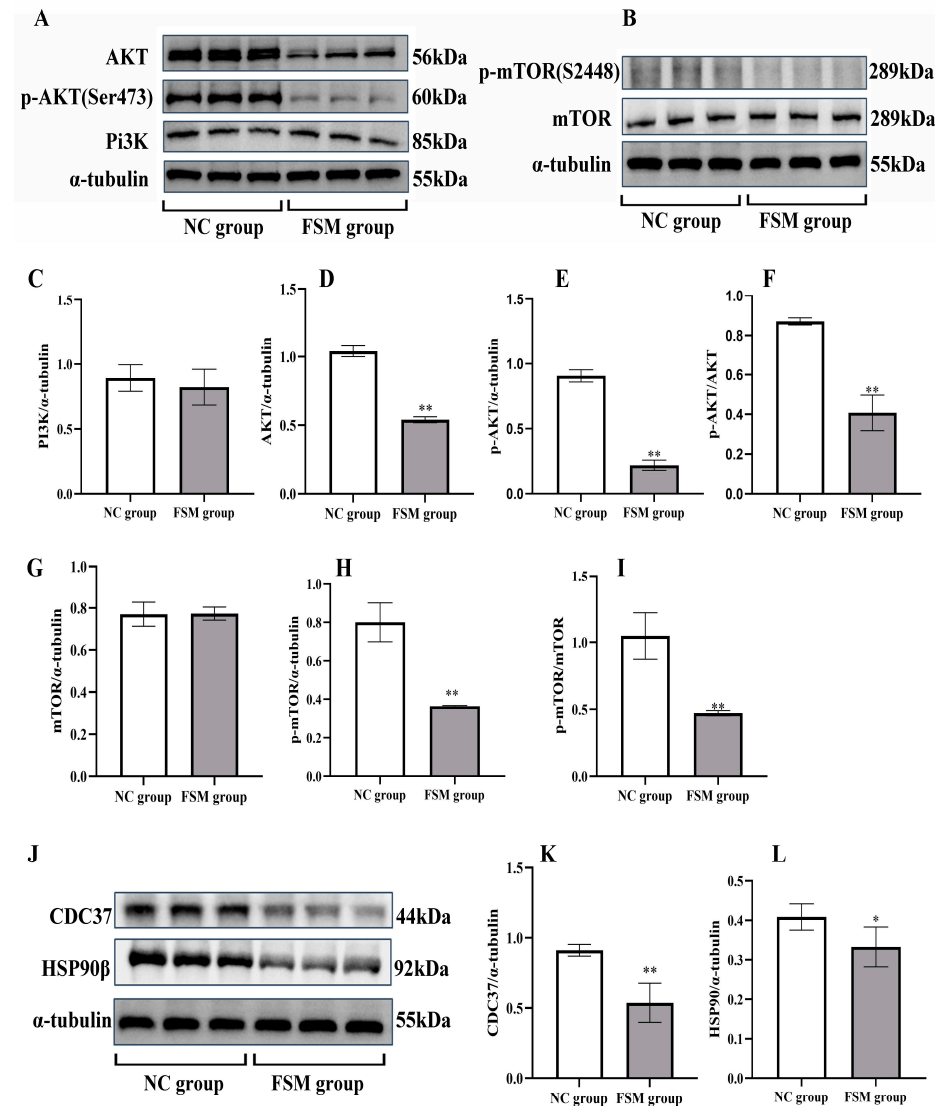
Figure 6. The expressions of PI3K/AKT/mTOR pathway in the placenta of rats detected by western blotting assay. (**A**) Representative western blotting images of PI3K, AKT, and p-AKT; (**B**) Representative western blotting images of mTOR and p-mTOR. The protein expressions of PI3K (**C**), AKT (**D**), and p-AKT (**E**) determined by image J software (1.53n); (**F**) The p-AKT/AKT ratio calculated. The protein expressions of mTOR (**G**) and p-mTOR (**H**) determined by image J software (1.53n); (**I**) The p-mTOR/mTOR ratio calculated. (J) Representative western blotting images of CDC37 and HSP90β. The protein expressions of CDC37 (**K**), and HSP90β (**L**) determined by image J software (1.53n). Results presented as means ± SD ($n = 6$). ** $p < 0.01$ and * $p < 0.05$ versus ONC group.

2.9. The Impact of Maternal Stress on Placental Cdc37 and HSP90β Protein Expression

The pathway analysis showed that the expressions of CDC37 and HSP90β proteins in PI3K-Akt signaling pathway decreased significantly in the FSM group. The western blotting assay was employed to verify these results, as shown in Figure 6. The expression of placental Cdc37 (Figure 6J,K) and HSP90β chaperones (Figure 6J,L) were significantly decreased in the group exposed to prenatal stress. These results were consistent with the proteome detection outcomes. Our results suggest that the decreased expressions of Cdc37

and HSP90β chaperones in the placenta may affect placental development via inhibiting cell signaling of PI3K/AKT.

In conclusion, we demonstrated that prenatal fear stress induced decreases in the expressions of Cdc37 and HSP90β chaperones in the placenta, further inhibiting the PI3K/AKT/mTOR pathway (Figure 7). This disruption in placental signaling is likely to impact fetal growth and development.
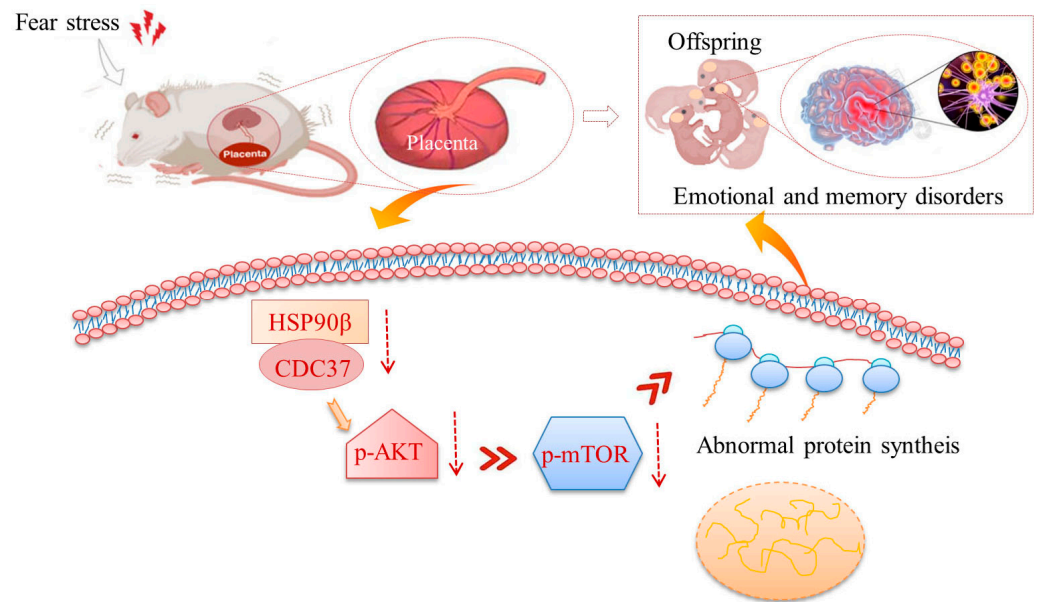
Figure 7. Schematic diagrams for prenatal stress-induced placental damage. Prenatal fear stress induces down-regulation of PI3K/AKT/mTOR pathway in placenta. These abnormalities in protein expression might damage the barrier function of the placenta and thereby cause abnormal development in the offspring.

3. Discussion

We investigated the effects of chronic fear stress on placental proteins expression in pregnant rats, iTRAQ-based proteomics analysis was employed for obtaining the unbiased profiling data. These findings are instrumental in elucidating the mechanisms underlying placental injury caused by chronic fear stress in pregnant rodents. Our previous research has demonstrated that such stress not only precipitates emotional disturbances in the dams but also impairs the growth, development, and cognitive abilities of their offspring [2]. Similar results have been reported by Brannigan et al. [13], who observed that offspring exposed to maternal stress during gestation exhibited an elevated predisposition to psychiatric conditions in later life. This mechanism is attributed to elevated corticosterone levels in the maternal plasma. Chronic exposure of the placenta to heightened glucocorticoid concentrations results in diminished 11β-HSD2 activity, thereby facilitating a substantial increase in corticosterone levels reaching the fetal circulation, which in turn affects fetal development [14]. The placental barrier is crucial for safeguarding the fetus from deleterious exposures throughout pregnancy. Our initial investigations demonstrated that stress induced by fear during gestation elicits modifications in m6A methylation within the mother's placental tissue [7]. However, the specific proteins within the placenta that may undergo abnormal expression due to such alterations remain undefined. To date, prior research has yet to provide an exhaustive comprehension of the extensive interconnection between prenatal stress and placental protein expression. Proteomic inquiries are imperative to deciphering the potential biological correlations between prenatal stress and pathological alterations in the placenta.

In this study, pregnant rats were subjected to prolonged fear-induced stress throughout their gestational period by observing the application of electrical stimulation to male

counterparts. Three different stress-response phenotypes and the levels of stress hormones of the prenatal fear stress rat model were evaluated. The results demonstrated that the rats that were subjected to fear-induced psychological stress manifested anhedonia-like behavior, evidenced by a diminished preference for sucrose water compared to the control rats. Moreover, these rats exhibited increased immobility during the TST and a reduced propensity for exploration in the OFT, indicative of behavioral depression. Additionally, elevated serum stress hormone concentrations confirmed the stress condition in the pregnant rats. Collectively, the prenatal fear stress rat model, induced by the observation of electrical stimulation in male rats, serves as an appropriate animal model for studying psychological stress during pregnancy. To investigate the correlation between prenatal fear stress and placental damage, as well as to elucidate the detrimental impacts of such injuries on offspring development, we conducted assessments of the progeny's behavioral patterns. Our investigation revealed that progeny of rats subjected to fear stress manifested growth retardation, accompanied by deficits in learning and memory functions. These outcomes were consistent with our previous reports [2], thereby affirming the consistency and reliability of our methodology. A significant benefit of this model is that it is an exclusively psychological stress model. The stressor itself does not result in severe physical harm to the pregnant rats, such as exposure to humidity, starvation, pain, or other adverse stimuli that could potentially influence fetal development. Consequently, the psychological stress model employed in our study is an optimal choice for assessing maternal stress during pregnancy, offering critical insights into the pathogenesis of Emotion-Caused Disease Theory during this critical period.

Placental tissue is integral to the oxygen and nutrient transfer between mother and fetus, facilitating essential maternal–fetal interactions. The functions of the placenta extend beyond its primary role, encompassing scavenging and endocrine activities. It secretes neuroactive signaling molecules with endocrine, paracrine, and autocrine effects, regulating the activity of other endocrine glands and thereby influencing maternal adaptation to pregnancy [15]. As the physiological conduit between mother and fetus, the placenta serves as a critical barrier against harmful prenatal exposures. Nevertheless, psychological stress during pregnancy may compromise these protective mechanisms, potentially impairing fetal physiological and neural development [8]. Our results illustrated that fear stress in pregnant rats during the gestation period might induce a pathological hypercoagulable state and reduce blood oxygen saturation. These hematological pathological changes in pregnant rats would impact the placental O2 and nutrient transfer at the maternal–fetal interface, and ultimately lead to abnormal embryonic development. Normal pregnancy is characterized by a physiological hypercoagulable state, which serves a protective role in mitigating bleeding complications during parturition [16]. Exaggerated hematological pathological changes in pregnant rats may lead to placental ischemia, subsequently impacting the gas exchange and nutrient transport between mother and fetus [17]. Chronic stressors, such as occupational strain, posttraumatic stress disorder, and psychological distress from depressive and anxiety symptoms, activate the sympathoadrenal medullary system, resulting in a chronic low-grade hypercoagulable state [18,19]. In the context of pregnancy, when such stressors arise, the hematological pathological alterations are magnified in pregnant rats, potentially precipitating placental ischemia. This condition may result in compromised maternal–fetal circulation, thereby predisposing the fetus to preeclampsia, fetal growth restriction, abruptio placentae, intrauterine death, and stillbirth [20–22]. These results indicate that maternal exposure to fear stress throughout pregnancy may elicit a pathological hypercoagulable condition in pregnant rats, potentially diminishing placental functionality and ultimately impacting the ontogenetic progression of the embryos. The results may help with the development of strategies for the diagnosis and prevention of diseases caused by prenatal psychological stress.

The atypical hypercoagulable condition not only impacts the interchange of gases and nutritional substances between the mother and the fetus, but also alters the structural integrity of the placenta itself [23]. Consequently, we conducted morphological assessments

of the placenta utilizing H&E staining and Masson staining techniques. Additionally, we evaluated fetal weight, placental weight, and placental efficiency as indicators of placental anomalies. Our morphological findings revealed an accumulation of red blood cells within the placental vasculature in the FSM group, a condition potentially linked to the pathological hypercoagulability observed in the pregnant rats. Furthermore, there was a significant reduction in fetal weight, placental weight, and placental efficiency observed in rats subjected to psychological stress. These findings corroborate our hypothesis that chronic fear stress during pregnancy induces pathological hypercoagulability in pregnant rats, thereby mediating placental ischemia and inflicting substantial harm to neonates.

To elucidate the impact of maternal psychological stress on placental functionality, our research entailed a comprehensive proteomic examination of placental tissue to discern the biological underpinnings associating stress with pathological changes in the placenta. The results revealed that 287 proteins exhibited marked differential expression between the two groups. When we entered the glucocorticoid receptor gene NR3C1 along with 287 differentially expressed proteins into the STRING database for protein interaction analysis (STRING score = 0.4, FDR stringency = 0.01), it was discovered that NR3C1 can interact with two of these genes (stip1 and ptges3), suggesting that their expression may be modulated by the glucocorticoid receptor signaling pathway. Bioinformatics analysis revealed that these differential proteins were mainly enriched in blood coagulation, coagulation, fibrin clot formation, rRNA processing, translation, protein folding, protein stabilization, oxygen transport, and other biological processes of the placenta. The molecular functions of the DEPs were mainly involved in protein binding, RNA binding, and a structural constituent of the ribosome. The pathway enrichment analyses of the DEPs were mainly involved in ECM-receptor interaction and PI3K-Akt signaling pathway. PPI analysis revealed that 39 hub genes may play a significant role in the impairment of placental function due to pregnancy-related stress. Subsequent analysis indicated that among these genes Fgg, Alb, Vtn, Gnaq, Tcp1, cct5, Hsp90ab1, and eEF2 were regulated by the PI3K-Akt signaling pathway.

Phosphoinositide 3 kinase (PI3K) serves as a pivotal molecule in cellular signal transduction, with its principal downstream effector being the serine/threonine-protein kinase, protein kinase B (AKT) [24]. PI3K exhibits dual enzymatic activities, functioning as both a lipid kinase and a protein kinase. Activation of the PI3K signaling pathway leads to an increase in the production of PIP3, which subsequently associates with the intracellular signaling protein AKT, bearing a PH2 domain, and elevates its phosphorylation status. Phosphorylated AKT (p-AKT) is capable of phosphorylating the tuberous sclerosis complex (TSC1/2), thereby facilitating the release of RHEB and the subsequent activation of the mammalian target of rapamycin (mTOR) [25]. mTOR, a key cellular signaling molecule, influences cytokine expression, transcription, and protein synthesis, and governs cellular processes such as growth, autophagy, and apoptosis. As a serine/threonine protein kinase, mTOR can either complex with the rapamycin-associated TOR (RAPTOR) protein to form mTOR complex 1 (mTORC1) or with the rapamycin-insensitive companion of mTOR (RICTOR) to form mTOR complex 2 (mTORC2). Conditions of hypoxia or energy deficiency can result from the inhibition of mTOR and the suppression of protein translation. In mice deficient in either mTOR or RAPTOR, fetal demise occurs around the peri-implantation period, highlighting the crucial role of mTOR in early placental and embryonic development [26]. Fetal growth is intimately associated with modifications in the placental mechanistic targeting of mTOR signaling, with reduced signaling observed in fetal growth restriction and increased signaling in fetal overgrowth [27]. It has been postulated that the placenta orchestrates a complex integration of maternal and fetal nutritional signals with intrinsic nutrient-sensing pathways to align fetal demand with maternal supply, regulating maternal physiology, placental growth, and nutrient transport, with trophoblast mTOR playing a central role in this homeostatic regulatory mechanism [28]. In the occurrence of an unusual insufficiency in uteroplacental blood perfusion, the placenta predominantly exhibits a suppression of both the mTORC1 and mTORC2 signaling axes. Following this suppression,

there is a decrement in the placental nutrient transport mechanisms, as evidenced by the diminished activity of amino acid and folate transporters. Concurrently, this is associated with a decline in mitochondrial activity and protein biosynthesis, cumulatively leading to a reduced fetal nutrient supply and ultimately culminating in intrauterine growth restriction (IUGR) [28]. Furthermore, the administration of corticosterone to pregnant rodents has been documented to suppress placental mTORC1, mTORC2, p-4EBP1, and p-Akt [29]. In this study, the protein expression levels of AKT, p-AKT, and p-mTOR in placental tissue were significantly reduced in the FSM group compared with those in the NC samples. These results lead us to speculate that placental PI3K/Akt/mTOR signaling pathway dysfunction plays a vital role in the process of placental dysfunction caused by maternal psychological stress.

In the context of untreated cellular environments, a significant proportion—approximately 30%—of Akt is found to be associated with a complex involving HSP90 and cdc37. This association is potentially pivotal for the maintenance of Akt stability, as indicated by reference [30]. The inhibition of cdc37 has been observed to weaken the PI3K/AKT kinase signaling pathways, which are integral to the regulation of the trophoblast cell cycle and proliferation, as documented in references [31,32]. The Hsp90 protein, encoded by the genes hsp90aa1 and hsp90ab1, corresponds to the Hsp90α and Hsp90β subtypes, respectively. Notably, the expression of Hsp90β exhibits a constitutive pattern, whereas Hsp90α expression is significantly elevated in response to cellular stress, as per reference [33]. Hsp90β is essential for mouse development, while Hsp90α plays a role in maintaining male fertility in adult mice, as stated in reference [34]. In this study, the expression levels of Cdc37 and HSP90β chaperones in placental tissue were significantly reduced in the FSM group when compared to those in the NC samples. These findings were in line with the proteome detection results. Our results imply that decreased expressions of Cdc37 and HSP90β chaperones in the placenta might impact placental development by inhibiting the cell signaling of PI3K/AKT.

In conclusion, we employed LC-MS and iTRAQ based proteomics to ascertain if fear stress in pregnant rats has an impact on placental proteomics. We discovered that fear stress during pregnancy elicited elevated glucocorticoid concentrations and pathological hypercoagulability, ultimately leading to the suppression of the placental PI3K-Akt signaling pathway. This disruption impacts a spectrum of placental biological processes, including rRNA processing, translation, protein folding, protein stability, and oxygen transport. Such dysfunctions may compromise the placental barrier function, potentially resulting in developmental abnormalities in the offspring.

4. Materials and Methods

4.1. Animal Care and Ethics Statement

A total of 30 female Wistar rats and 15 male Wistar rats aged 11 weeks and weighing 230–260 g [Purchased from Beijing weitonglihua Experimental Animal Technology Co., Ltd., Beijing, China, license number: SCXK (Jing) 2016–0006] were housed in standard laboratory conditions (20 ± 3 °C, 45 ± 5% relative humidity, 12/12 h light/dark cycle) and were given access to food and water ad libitum. All experiments were approved by the Ethics Committee of Henan University of Chinese Medicine (Zhengzhou, China) under the regulations of National Institutes of Health guidelines for the care and use of laboratory animals.

4.2. Animal Treatment

4.2.1. Prenatal Fear Stress

All female rats and male rats were mated in a cage with the ratio of 2:1 according to our previous study [2]. Mating and gestation were estimated based on the presence of sperm in the vagina of female rats. After fertilization, 24 pregnant rats were randomly assigned to either the normal control (NC) or fear stress model (FSM) group, with 12 rats in each. The prenatal fear stress procedure was conducted according to our previous study [2].

Briefly, FSM pregnant rats were placed into an improved electric shock box to observe and listen to the traumatic event of male rats being subjected to electric stimulations for 20 days (Figure 8) [35–37]. Control pregnant rats were placed in the same situation but did not undergo the psychological fear stress procedure. In the NC group, the pregnant female rats were subjected to identical conditions; however, no galvanic stimulation was applied to the base of the apparatus for the box. Consequently, the male rats were not exposed to electrical currents and, as a result, did not manifest behaviors such as screaming or jumping, thereby failing to communicate any fear-related cues. In periods of fear stress, the pregnant female rats were raised in separate cages from the male rats.
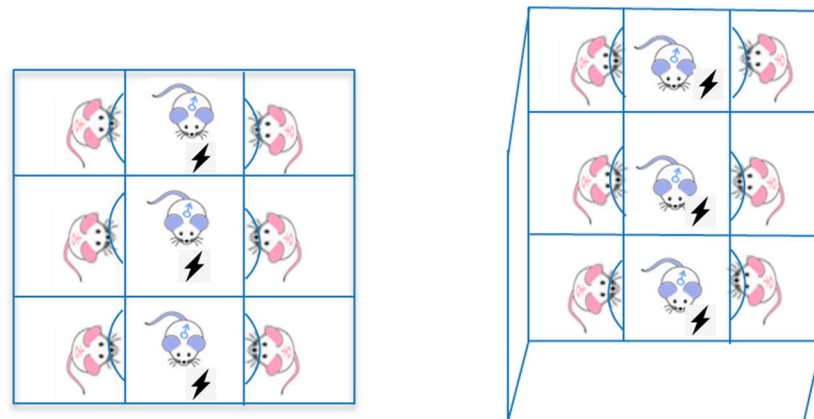
Figure 8. Fear stress schema illustration.

4.2.2. Stress State Assessment of Pregnant Rats

In the final week of gestation, the sucrose preference test (SPT), open field tests (OFT), and tail suspension test (TST) were administered to evaluate anxiety profiles in the pregnant rats [37,38]. Concurrently, serum ACTH and CORT concentrations were quantified on the 20th day of pregnancy using enzyme linked immunosorbent assay (ELISA) to assess stress hormone responses.

4.2.3. The Behavioral Assessment of the Offspring

Four pregnant rats gave birth naturally in each group, and 39 and 32 neonatal rats were obtained in the NC group and FSM group, respectively. The behavioral and developmental assessment of neonatal progeny was conducted according to our previous study (see Figure 9). Specifically, the chronological milestones of physical maturation of all pups in each dam, including the acquisition of surface righting reflexes and auditory startle reflexes, were meticulously documented. Furthermore, the onset of eye opening, incisor emergence, and auricular patency were meticulously recorded to ascertain the pups' physiological development and maturation. In addition, between postnatal days (PNDs) 21 and 27, 10 offspring rats (5 males and 5 females) were selected from each group for behavioral assessment; the SPT (PND 21–23), OFT (PND 21 a.m.), the Morris Water Maze (MWM, PND 23–27), and the TST (PND 21 p.m.) were administered to evaluate the offspring's anxiety levels and their cognitive learning and memory abilities.

4.3. Method of Behavioral Testing

4.3.1. Open Field-Test

The open field-test was conducted as follows [39]: rats were positioned in the central area of an open-field apparatus measuring 100 cm × 100 cm × 50 cm. The apparatus floor was segmented into 25 equivalent sections. The movement tracks of the rats were recorded via a video camera over a span of 5 min, with the apparatus being sanitized with alcohol between each trial.
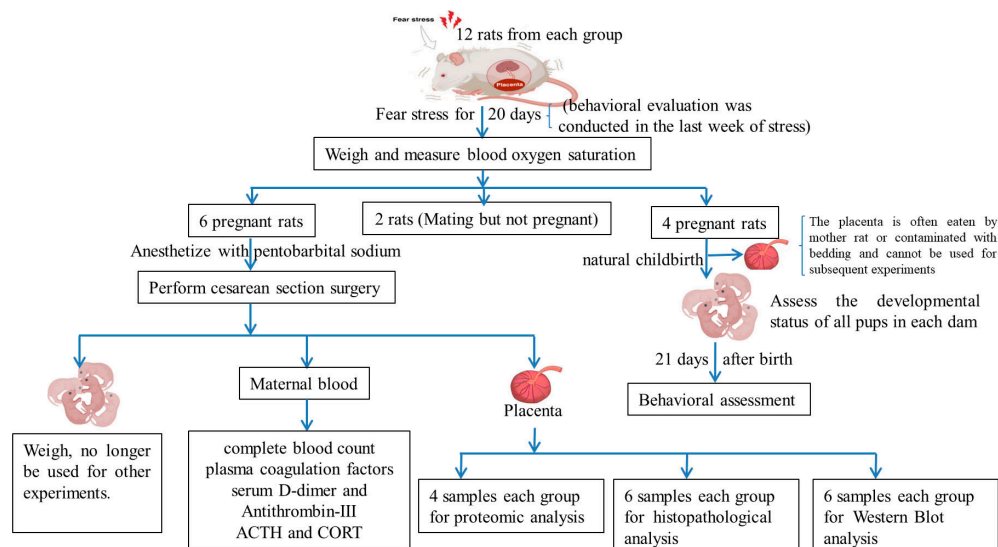
Figure 9. Schematic diagrams for the experimental protocol.

4.3.2. TST

The TST was performed in accordance with established methodologies [40]. Rats were hung by their tails for a period of 6 minutes. Immobility was defined as a complete lack of movement. The cumulative immobility time was recorded for the final 4 min of the 6-min session.

4.3.3. SPT

The SPT [40] was conducted as follows: Initially, each rat was individually housed in a single-cage environment, and acclimated to a 1% sucrose solution for the duration of 24 h. Subsequently, they underwent a 12-h fast from both food and water. On the third day of the experimental protocol, pairs of identical bottles containing 1% sucrose solution and tap water were placed in each cage concurrently. After an hour, the positions of the two bottles were interchanged. One hour later, the remaining volumes of the liquids were quantified. The percentage of sucrose preference was measured as follows: sucrose preference = sucrose consumed/(sucrose consumed + tap water consumed).

4.3.4. MWM

The MWM Test was performed according to a previously reported protocol [41]: The water maze was a black circular pool (100 cm in diameter, 60 cm in height) with a stable platform positioned 1 cm beneath the water surface. Prior to testing, the maze was filled with tap water at a temperature of 25–27 °C and rendered opaque by the addition of a non-toxic white paint. The experiment comprised two sequential phases: place navigation (initial training) and spatial probe (the Space Exploration Test). During the initial training phase, the platform was situated centrally in the north quadrant. Each rat was placed in the pool, oriented towards the wall, at one of four starting points (north, south, east, and west) in a semirandom sequence, and allowed 120 s to locate the submerged platform. Rats that voluntarily found the platform were allowed a 5-s stay, whereas those that failed to do so within the allocated time were gently directed to the platform and held there for 30 s. Each rat underwent four trials daily over a period of 4 consecutive days, the time spent by the rats to reach the platform (escape latency times) were recorded. Following the 4-day training regimen, the spatial probe test was performed to evaluate memory retention. On the 5th day, the platform was removed, and each rat was released into the water from the quadrant opposite to the platform's previous location, with a 90-s search period. The frequency of each rat's crossings over the original platform position, swimming velocities, and the duration spent in the target quadrant were meticulously documented and analyzed using a video-tracking system (CG-400 Image Acquisition System; Institute

of Materia Medica, Chinese Academy of Medical Sciences, Shanghai, China). Post-trial, the rats were dried and maintained at a comfortable temperature before being returned to their enclosures.

4.4. Sample Preparation

On the 20th day of pregnancy, six pregnant rats in each group, after a 12-h fast, were subjected to fear stress for 30 min daily, followed by immediate anesthesia with pentobarbital sodium (50 mg/kg, intraperitoneally). Blood samples were collected from the abdominal aorta; the K2-EDTA anticoagulated whole blood, sodium citrate anticoagulated plasma, and serum were collected. All blood samples were procured within a 2-h window following the rats' exposure to fear stress. Sodium citrate anticoagulated plasma and serum were stored frozen, and all biochemical tests were completed within 1 month. The fetuses and placentas were swiftly separated, and the number of litters was recorded, and then weighed using a digital scale. Additionally, the diameters and thicknesses of the placentas were manually measured using a caliper (Mitutoyo, Kanagawa, Japan). Placental efficiency was expressed as the ratio of fetal weight to placental weight. Three placentas were randomly selected from each dam, and stored in liquid nitrogen, used for Western blot analysis and proteomic analysis. Each placenta was randomly selected from the respective dams and subsequently immersed in a 4% paraformaldehyde solution at a temperature of 4 °C for a duration of one week to facilitate H&E staining procedures. In the experimental cohort, the remaining pregnant rats underwent spontaneous parturition. On the 20th day of gestation, the blood oxygen saturation levels in these rats were assessed. Furthermore, the oxygen saturation in their progeny was quantified on PND 1 and PND 21 utilizing a PC100SEV animal oximeter (Wuhan Weisi Biotechnology Co., Ltd., located in Wuhan, China).

4.5. Biochemical Assay

Utilizing K2-EDTA anticoagulated whole blood, complete blood count (CBC) determinations were performed on the day of sample collection via an Mairui animal automatic blood cell analyzer (BC-2800vet, Shenzhen, China). Concurrently, plasma coagulation factors were assayed using in vitro diagnostic kits (cat. no. R01002, R01102, R01202, and R01302, Redu Life Sciences Co., Ltd., Shenzhen, China). Additionally, serum D-dimer and Antithrombin-III levels were quantified by enzyme linked immunosorbent assay (cat. no. JL21114, JL15661, Shanghai Jianglai Biotechnology Co., Ltd., Shanghai, China), along with ACTH and CORT concentration measurements (cat. no. H097-1-2, H205 Shanghai Jianglai Biotechnology Co., Ltd., Shanghai, China) to assess stress hormone responses and the functionality of both coagulation and anticoagulant systems.

4.6. Histological Examination

The placental tissues within a 3 mm radius from the insertion point of the umbilical cord were selected. The placenta tissues were dehydrated with graded alcohol series (80%, 95%, and 100%) and embedded in paraffin. They were then sliced into serial transverse 4-μm-thick sections, six slices for each sample. The sections were stained with hematoxylin & eosin (H&E) and Ponceau-s & aniline blue (Masson).

4.7. Proteomic Analysis
4.7.1. Protein Extraction

Placental samples with a diameter of 5 mm around the umbilical cord were isolated, approximately 100 mg of the placental sample from each rat was homogenized in liquid nitrogen and mixed well with $6 \times$ volume of chilled TCA-acetone (500 mL acetone, 50 g TCA), and precipitated at -20 °C for about 2 h. After centrifugation at 4 °C and $20,000 \times g$ for 30 min, the supernatant was discarded, and the precipitate was mixed well with 4 volume equivalents of chilled acetone, precipitated at -20 °C for 30 min, centrifuged at 4 °C and $20,000 \times g$ for 30 min again. The precipitate was dissolved with lysis buffer (8 M urea,

30 mM HEPES, 1 mM PMSF, 2 mM EDTA, 10 mM DTT) and sonicated at 180 W for 5 min (pulse on 2 s pulse off 3 s for each time). The mixture was centrifuged at 4 °C and 20,000× g for 30 min again, the supernatant was collected and added to DTT (10 mM), the mixture was incubated at 56 °C for 1 h, then added to IAM (55 mM) and incubated in darkness for 1 h, then 6 × volume of chilled acetone was added and precipitated at −20 °C for at least 3 h. Having subsequently undergone centrifugation at 4 °C and 20,000× g for 20 min, the precipitate was collected and redissolved in 700 µL of dissolution buffer (50% TEAB, 0.1% SDS) and sonicated at 180 W for 3 min. After centrifugation at 4 °C and 20,000× g for 30 min, the supernatant was collected and the protein concentrations were quantified using the Bradford method (Pierce™ Coomassie [Bradford] Protein Assay Kit, ThermoFisher, Waltham, MA, USA).

4.7.2. Protein Digestion and Peptide iTRAQ Labeling

Proteins (100 µg per sample) were added to the dissolution buffer (50% TEAB, 0.1% SDS) and digested with trypsin. This was then freeze-dried and redissolved with 30 µL dissolution buffer (50% TEAB, 0.1% SDS). The tryptic peptides were labeled with an iTRAQ®Reagent-8 Plex Multiplex Kit (Applied Biosystems, Waltham, MA, USA), following the manufacturer's instruction. The samples of NC group were labeled with iTRAQ reagent 113, 114, 115, 116, and the samples of FSM group were labeled with iTRAQ reagent 117, 118, 119, 121, respectively (Table 3). The labeled samples were incubated at room temperature for 2 h, the reaction was terminated by the addition of 10 × volume of dilution [10 mM KH2PO4, 25% acetonitrile (ACN), pH = 3.0], centrifuged at 4 °C and 15,000× g for 10 min, the supernatants were then collected and pooled. The peptides were preliminarily separated by strong cation exchange (SCX) chromatographic-HPLC. The chromatography conditions were: the labeled peptides were loaded onto an SCX chromatographic column (Luna SCX 250 × 4.60 mm 100 Å, phenomenex) and equilibrated in 100% solution A for 10 min, followed by a fast elution. The elution reagents consisted of the solvent A (10 mM KH2PO4 in 25% ACN, pH = 3.0) and solvent B (2 M KCL, 10 mM KH2PO4 in 25% ACN, pH = 3.0, flow rate = 1 mL/min). The gradients were as follows: 0% B for 45 min; 0–5% B for 1 min; 5–30% B for 10 min; 30–50% B for 5 min; 50% B for 5 min; 50–100% B for 5 min; and 100% B for 10 min. After 46 min of elution, the fractions were collected at a rate of 1 tube/min, and the fractions with few peaks were combined. The fractions were desalted using a C18 column (strata-X C18, phenomenex), lyophilized, and dissolved in 0.1% formic acid for LC-MS/MS analyses.

Table 3. Peptide segment labelling information.

	Sample Name	Labels Information
NC group	N1	113
	N2	114
	N3	115
	N4	116
FSM group	M1	117
	M2	118
	M3	119
	M4	121

4.7.3. LC-MS/MS Analyses

The peptides in each fraction were loaded onto an Acclaim PePmap C18-reversed phase column (3 µm, 75 µm × 2 cm 100 Å, Thermo Scientific, Waltham, MA, USA) and connected with a reversed phase C18 column (5 µm, 75 µm × 10 cm 300 Å, Agela Technologies, Tianjin, China) for separation, and then gradiently eluted with 5–80% (*v*/*v*) ACN in 0.1% formic acid for 65 min at 300 nL/min. The peptide fractions were analyzed using a Q Exactive mass spectrometer (Thermo Fisher Scientific, MA, USA). The detection method was positive ion, the capillary voltage was 1800 V, and the capillary temperature was

300 °C. The acquisition ranges were 350–2000 m/z at a resolution of 70,000 for the MS. The resolution for MS/MS scan was set to 17,500 with a minimum signal threshold at 1×10^5 and isolation width at 2 m/z.

4.7.4. Protein Identification and Quantification

The identification and quantification of peptides and proteins were constituted using the ThermoFisher Proteome Discoverer (version 1.3) tool with Sequest HT search engine based on the UniProt rat database. The user-defined search parameters were set as follows: trypsin; missed cleavages, two; fixed modifications, iTRAQ 8plex on N-term and Lys, and Carbamidomethylation on Cys; variable modification, Oxidation on Met, deamidation on Asn and Gln, and Pyro-Glu, and acetylation on protein N-term; precursor mass tolerance of 15 ppm; fragment mass tolerance of 0.05 Da. The false discovery rate for peptide spectrum matching in protein and peptide identification with the filter module is below 0.01, necessitating further data screening. The ion quantifiers, along with peptide and protein quantifier nodes, were employed to compute and quantify the relative proportions of peptides and proteins in the sample. Each identified protein involved at least one unique peptide. After these procedures, we obtained the quantitative results of protein expression data. After weighing and normalizing by the median ratio, the resultant ratio data were subjected to statistical evaluation via a two-tailed Student's t-test to verify the significance of the differences between the two groups: the NC group and the FSM group. Proteins with a change greater than 1.2-fold and a p-value lower than 0.05 were regarded as DEPs.

4.7.5. Bioinformatics Analysis

The protein–protein interaction network was constructed by the STRING database [42]. The functional annotation of DEPs was performed using the Gene Ontology (GO) database. The prediction of the significant pathways was carried out with Kyoto Encyclopedia of Genes and Genomes (KEGG) database [43–45]. Cytoscape 3.7.2 software was used to visualize the results.

4.8. Western Blot Analysis

The total proteins from the placenta was extracted using RIPA lysis buffer (50 mM Tris [pH 7.4], 150 mM NaCl, 1% Triton X-100, 1% sodium deoxycholate, 0.1% SDS) with PMSF, protease inhibitor and a phosphatase inhibitor. A BCA protein quantitative detection kit (Jiangsu Meimian Industrial Co., Ltd., Changzhou, China) was used to determine the protein content. The protein was separated with SDS-PAGE and transferred to PVDF membranes with electrophoresis systems (Bio-Rad 1645050, Hercules, CA, USA). The PVDF membranes were blocked with 5% (*w/v*) skimmed milk powder for 2 h and incubated at 4 °C overnight with the following primary antibodies anti-PI3K (Cat No.GB11525-100, Servicebio, Wuhan, China), anti-AKT (Cat No.GB15689-100, Servicebio, Wuhan, China), anti-phospho-AKT (p-AKT, Cat No.GB 150002-100, Servicebio, Wuhan, China), anti-mTOR (Cat No.GB111840-100, Servicebio, Wuhan, China), Phospho-mTOR (p-mTOR, Cat No.67778-1-ig, Proteintech, Wuhan, China), anti-CDC37 (Cat No.66420-1-ig, Proteintech, Wuhan, China) anti-HSP90β (Cat No.GB111280, Servicebio, Wuhan, China), and anti-α-tubulin (Cat No.GB15201-100, Servicebio, Wuhan, China). After being washed with 1× TBST solution (Servicebio, Wuhan, China) three times, the membranes were incubated with HRP-labelled secondary antibodies (Servicebio, Wuhan, China). A gel imaging system (Thermo Fisher Scientific, MA, USA) and Image J Software were used for imaging and statistical analysis. α-tubulin was used as an internal control to ensure equal protein loading.

4.9. Statistical Analyses

Measurement data was presented as means ± SDs, and the statistical analyses were performed using SPSS 21.0 statistical software (IBM, Armonk, NY, USA). The escape latency of offspring was analyzed using repeated-measures ANOVA. The offspring's other

behavioral results were analyzed through Two-Way ANOVA. The other measurement data were analyzed using independent *t*-test. $p < 0.05$ was considered statistically significant.

5. Conclusions

Prenatal fear stress induced the inhibition of the cellular signal transduction of placental PI3K/AKT/mTOR, which affected biological processes such as rRNA processing, translation, protein folding, protein stability, and oxygen transport in the placenta. The results suggested that fear stress during pregnancy elicited elevated glucocorticoid concentrations and pathological hypercoagulability, ultimately leading to the suppression of the placental PI3K-Akt signaling pathway. This disruption impacts a spectrum of placental biological processes, including rRNA processing, translation, protein folding, protein stability, and oxygen transport. Such dysfunctions may compromise the placental barrier function, potentially resulting in developmental abnormalities in the offspring.

Supplementary Materials: The following supporting information can be downloaded at: https://www.mdpi.com/article/10.3390/ijms25189978/s1.

Author Contributions: Writing—original draft preparation, Y.L.; writing—review and editing, Y.L. and L.Y.; data curation, Y.L., H.M. and J.H.; methodology, T.Z., Z.D. and Y.J.; visualization, Y.L., L.Y., G.L., J.Z. and P.C.; funding acquisition, Y.L., L.Y. and J.H. All authors have read and agreed to the published version of the manuscript.

Institutional Review Board Statement: All experiments were approved by the Ethics Committee of Henan University of Chinese Medicine (Henan, China) under the regulations of National Institutes of Health guidelines for the care and use of laboratory animals. (Protocol code: DWLLGZR202202061. Date of approval: 28 February 2022).

Informed Consent Statement: Not applicable.

Data Availability Statement: The original contributions presented in the study are included in the article/supplementary material; further inquiries can be directed to the corresponding author/s.

Conflicts of Interest: The authors declare no conflicts of interest.

Appendix A

Table A1. Upregulated proteins in the placenta.

Accession	Protein Names
P06238	Alpha-2-macroglobulin (A2m)
D4A2F1	Agrin (Agrn)
P02770	Serum albumin (Alb)
A0A0G2JX94	Protein Amot (Amot)
P36633	Amiloride-sensitive amine oxidase [copper-containing] (Aoc1)
P29975	Aquaporin-1 (Aqp1)
P06685	Sodium/potassium-transporting ATPase subunit alpha-1 (Atp1a1)
Q63377	Sodium/potassium-transporting ATPase subunit beta-3 (Atp1b3)
M0RCA6	Advillin (Avil)
Q63514	C4b-binding protein alpha chain (C4bpa)
Q9R0T4	Cadherin-1 (Cdh1)
Q91XU8	Phosphatidate cytidylyltransferase 2 (Cds2)
Q4QQU3	Carcinoembryonic antigen-related cell adhesion molecule 11 (Ceacam11)

Table A1. *Cont.*

Accession	Protein Names
Q4V8J0	Carcinoembryonic antigen gene family 4 (Cgm4)
A0A0G2JZF2	CAP-Gly domain-containing linker protein 2 (Clip2)
Q6Q0N1	Cytosolic non-specific dipeptidase (Cndp2)
F1LR02	Procollagen, type XVIII, alpha 1, isoform CRA_a (Col18a1)
F1M6Q3	Protein Col4a2 (Col4a2)
D3ZUL3	Protein Col6a1 (Col6a1)
Q63768	Adapter molecule crk (Crk)
P14841	Cystatin-C (Cst3)
P00787	Cathepsin B (Ctsb)
Q32PZ8	Ctsq protein (Ctsql2)
Q9QUR2-2	Isoform 2 of Dynactin subunit 4 (Dctn4)
A0A0G2K719	Protein Ddx3x (Ddx3x)
Q6P725	Desmin (Des)
Q9EPB1	Dipeptidyl peptidase 2 (Dpp7)
D4A269	Uncharacterized protein (ENSRNOG00000005630)
A0A0G2JUY4	Uncharacterized protein (ENSRNOG00000050102)
D3ZF97	Protein Erlec1 (Erlec1)
D3ZVK6	Protein LOC103691893 (Erv3)
D3ZJ32	Protein Esyt2 (Esyt2)
G3V843	Prothrombin (F2)
P07483	Fatty acid-binding protein, heart (Fabp3)
P55053	Fatty acid-binding protein, epidermal (Fabp5)
P25093	Fumarylacetoacetase (Fah)
B2GV94	Fam134c protein (Fam134c)
B2GUZ9	Fam49b protein (Fam49b)
D3ZQ25	Fibulin-1 (Fbln1)
G3V9M6	Fibrillin 1, isoform CRA_a (Fbn1)
P06399	Fibrinogen alpha chain (Fga)
P14480	Fibrinogen beta chain (Fgb)
P02680-2	Isoform Gamma-A of Fibrinogen gamma chain (Fgg)
A0A0H2UHR7	Filamin-C (Flnc)
P04937	Fibronectin (Fn1)
A0A0G2K0A1	Protein Fndc3c1 (Fndc3c2)
D3ZAL7	Protein Gab1 (Gab1)
P50442	Glycine amidinotransferase, mitochondrial (Gatm)
P54313	Guanine nucleotide-binding protein G(I)/G(S)/G(T) subunit beta-2 (Gnb2)
F1LQQ8	Beta-glucuronidase (Gusb)
O35952-2	Isoform 2 of Hydroxyacylglutathione hydrolase, mitochondrial (Hagh)
D4A3K5	Histone H1.1 (Hist1h1a)
D3ZBN0	Histone H1.5 (Hist1h1b)
P27881	Hexokinase-2 (Hk2)
Q6P747	Heterochromatin protein 1-binding protein 3 (Hp1bp3)
Q6AYS8	Estradiol 17-beta-dehydrogenase 11 (Hsd17b11)
Q5I0N4	Estradiol 17-beta-dehydrogenase 2 (Hsd17b2)
P0DMW0	Heat shock 70 kDa protein 1A (Hspa1a)
F1LTJ5	Uncharacterized protein (Hspg2)
B0BNJ2	CEA-related cell adhesion molecule 12 (Predicted) (Igfl3)
P20761	Ig gamma-2B chain C region (Igh-1a)
D3ZCG9	Integrin alpha 3 variant A (Itga3)
M0R961	Far upstream element-binding protein 2 (Khsrp)
Q70AM4	Kinesin-like protein (Kif13b)
Q5PQU1	Kininogen 1 (Kng1)
P08932	T-kininogen 2 (KNT2)
G3V779	Ladinin (Predicted), isoform CRA_b (Lad1)
F1MAN8	Laminin, alpha 5, isoform CRA_a (Lama5)
M0R6K0	Laminin subunit beta-2 (Lamb2)
F1MAA7	Protein Lamc1 (Lamc1)

Table A1. *Cont.*

Accession	Protein Names
Q99MZ8	LIM and SH3 domain protein 1 (Lasp1)
G3V8L3	Lamin A, isoform CRA_b (Lmna)
Q4V799	Similar to solute carrier family 7 (Cationic amino acid transporter, y+ system), member 3 (LOC292543)
A0A0G2JYK0	Protein LOC299282 (LOC299282)
A0A0G2JU68	Protein LOC304903 (LOC680415)
Q5BK33	p55 protein (LOC691642)
A0A0G2JYI0	Protein Lrba (Lrba)
P28494	Alpha-mannosidase 2 (Man2a1)
Q5M7W5	Microtubule-associated protein 4 (Map4)
F1LMW7	Myristoylated alanine-rich C-kinase substrate (Marcks)
D3ZBP4	Protein-methionine sulfoxide oxidase MICAL1 (Mical1)
A0A0H2UHX5	Neprilysin (Mme)
D3ZGE2	Myeloperoxidase (Mapped) (Mpo)
Q9Z1W6-4	Isoform 4 of Protein LYRIC (Mtdh)
Q63355	Unconventional myosin-Ic (Myo1c)
Q6JE36	Protein NDRG1 (Ndrg1)
Q6P756	Adaptin ear-binding coat-associated protein 2 (Necap2)
F1LM84	Nidogen-1 (Nid1)
F1LZB6	Protein Nrk (Nrk)
D3ZZ80	Obscurin-like protein 1 (Obsl1)
P20717	Protein-arginine deiminase type-2 (Padi2)
G3V6S1	PRKC apoptosis WT1 regulator protein (Pawr)
Q62785	28 kDa heat- and acid-stable phosphoprotein (Pdap1)
Q9Z1Z9	PDZ and LIM domain protein 7 (Pdlim7)
Q5I0D7	Xaa-Pro dipeptidase (Pepd)
Q6P742	Proteolipid protein 2 (Plp2)
P85973	Purine nucleoside phosphorylase (Pnp)
D3ZS72	Protein Prex1 (Prex1)
P09320	Prolactin-4A1 (Prl4a1)
G3V850	Prolactin-7A2 (Prl7a3)
A0A0G2JTQ7	Prolactin-8A7 (Prl8a7)
Q4V883	Protein Psg16 (Psg16)
Q4V8K0	Pregnancy-specific glycoprotein 29 (Psg29)
P06302	Prothymosin alpha (Ptma)
O88902	Tyrosine-protein phosphatase non-receptor type 23 (Fragment) (Ptpn23)
G3V8L9	Polymerase I and transcript release factor (Ptrf)
Q1EG89	Myocardial ischemic preconditioning associated protein 7 (Pxn)
F1LSW7	60S ribosomal protein L14 (Rpl14)
P61314	60S ribosomal protein L15 (Rpl15)
P62718	60S ribosomal protein L18a (Rpl18a)
B2RZD4	60S ribosomal protein L34 (Rpl34)
B0K031	60S ribosomal protein L7 (Rpl7)
P62250	40S ribosomal protein S16 (Rps16)
D3ZDU2	Protein Rptor (Rptor)
D3Z8L7	Ras-related protein R-Ras (Rras)
Q9ERM8	Secretory carrier membrane protein 3 (Fragment) (Scamp3)
I3PMS6	Syndecan (Fragment) (Sdc4)
Q5XFW8	Protein SEC13 homolog (Sec13)
Q8VIF7	Selenium-binding protein 1 (Selenbp1)
A0A0H2UHI5	Protein LOC299282 (Serpina3n)
Q4G075	Leukocyte elastase inhibitor A (Serpinb1a)
Q5M7T5	Protein Serpinc1 (Serpinc1)
P20961	Plasminogen activator inhibitor 1 (Serpine1)
Q5EC47	Protein Slc13a4 (Slc13a4)
A0A0G2K2S2	Solute carrier family 2, facilitated glucose transporter member 1 (Slc2a1)
Q9EQ25	Sodium-coupled neutral amino acid transporter 4 (Slc38a4)
Q794F9	4F2 cell-surface antigen heavy chain (Slc3a2)

Table A1. *Cont.*

Accession	Protein Names
M0R6B7	Protein LOC100911874 (Slc40a1)
Q63016	Large neutral amino acids transporter small subunit 1 (Slc7a5)
D3ZUC9	Oxidative-stress responsive 1 (Predicted) (Snx8)
P12001	60S ribosomal protein L18 (Strn)
P48032	Metalloproteinase inhibitor 3 (Timp3)
Q4V8N0	Lipocalin 7, isoform CRA_a (Tinagl1)
D3ZA84	Protein Tln2 (Tln2)
D3ZF26	Protein Tnks1bp1 (Tnks1bp1)
Q4QRB4	Tubulin beta-3 chain (Tubb3)
Q5RJR2	Twinfilin-1 (Twf1)
P11232	Thioredoxin (Txn1)
D3ZF39	Protein Uap1 (Uap1)
D3ZFY8	Protein LOC100362142 (Ube2v1)
Q3KR94	Protein Vtn (Vtn)
P70490	Lactadherin (Ywhaq)
F1LVT2	Protein Zfp36l3 (Zfp36l3)
Q1RP74	Protein LOC100911774 (ZH14)
A0A0G2JSJ3	Solute carrier family 2 (Facilitated glucose transporter), member 3 (Slc2a3)

Table A2. Downregulated proteins in the placenta.

Accession	Protein Names
Q5XI64	Monoacylglycerol lipase ABHD6 (Abhd6)
P45953	Very long-chain specific acyl-CoA dehydrogenase, mitochondrial (Acadvl)
P51635	Alcohol dehydrogenase [NADP(+)] (Akr1a1)
P23457	3-alpha-hydroxysteroid dehydrogenase (Akr1c14)
A0A0G2K7X0	Acidic leucine-rich nuclear phosphoprotein 32 family member A (Anp32a)
Q07936	Annexin A2 (Anxa2)
Q4FZU6	Annexin A8 (Anxa8)
P43138	DNA-(apurinic or apyrimidinic site) lyase (Apex1)
D4A6C5	Protein Arhgap1 (Arhgap1)
Q9ER24	Ataxin-10 (Atxn10)
Q6P7P5	Basic leucine zipper and W2 domain-containing protein 1 (Bzw1)
Q68FQ0	T-complex protein 1 subunit epsilon (Cct5)
A0A0G2K3C1	Hsp90 co-chaperone Cdc37 (Cdc37)
G3V8V4	Longevity assurance homolog 2 (S. cerevisiae) (Cers2)
P10959	Carboxylesterase 1C (Ces1c)
D4A4T9	Cysteine and histidine-rich domain-containing protein 1 (Chordc1)
P61203	COP9 signalosome complex subunit 2 (Cops2)
D3ZI16	COP9 (Constitutive photomorphogenic) homolog, subunit 6 (Arabidopsis thaliana) (Predicted), isoform CRA_a (Cops6)
G3V936	Citrate synthase (Cs)
D3ZPR0	Chromosome segregation 1-like (S. cerevisiae) (Predicted) (Cse1l)
A0A0G2KBC4	Tyrosine-protein kinase receptor (Csf1r)
G3V8T4	DNA damage-binding protein 1 (Ddb1)
Q5U216	ATP-dependent RNA helicase DDX39A (Ddx39a)
B6DTP5	DEAD (Asp-Glu-Ala-Asp) box polypeptide 5 (Fragment) (Ddx5)
Q7M0E3	Destrin (Dstn)
P62630	Elongation factor 1-alpha 1 (Eef1a1)
B5DEN5	Eukaryotic translation elongation factor 1 beta 2 (Eef1b2)
Q68FR9	Elongation factor 1-delta (Eef1d)
P05197	Elongation factor 2 (Eef2)
A0A0G2K273	Eukaryotic translation initiation factor 3 subunit E (Eif3e)
Q6P3V8	Eukaryotic translation initiation factor 4A1 (Eif4a1)
P63074	Eukaryotic translation initiation factor 4E (Eif4e)
D4A8F2	Protein Rsu1 (ENSRNOG00000017595)

Table A2. *Cont.*

Accession	Protein Names
D4A6G6	Protein LOC100362339 (ENSRNOG00000018471)
D3ZZ95	60S ribosomal protein L36 (ENSRNOG00000031947)
P19132	Ferritin heavy chain (Fth1)
P02793	Ferritin light chain 1 (Ftl1)
Q5PQK2	Fusion, derived from t(1216) malignant liposarcoma (Human) (Fus)
P04276	Vitamin D-binding protein (Gc)
D4AE68	Guanine nucleotide binding protein, alpha q polypeptide, isoform CRA_a (Gnaq)
A0A0G2K0Z7	Glycerol-3-phosphate dehydrogenase, mitochondrial (Gpd2)
Q00715	Histone H2B type 1 (H2B1)
P01946	Hemoglobin subunit alpha-1/2 (Hba1)
A0A0G2JSV6	Protein Hba2 (Hba2)
A0A0G2JSW3	Hemoglobin subunit beta-1 (Hbb)
P11517	Hemoglobin subunit beta-2 (HBB2)
O88752	Epsilon 1 globin (Hbe1)
Q63066	Beta-globin chain (Fragment) (Hbg1)
G3V8R3	Protein Hbz (Hbz)
D3ZJ08	Histone H3 (Hist2h3c2)
P62804	Histone H4 (Hist2h4)
Q6URK4-2	Isoform 2 of Heterogeneous nuclear ribonucleoprotein A3 (Hnrnpa3)
Q9QX80	CArG-binding factor A (Hnrnpab)
G3V9R8	Heterogeneous nuclear ribonucleoprotein C (Hnrnpc)
P34058	Heat shock protein HSP 90-beta (Hsp90ab1)
P63039	60 kDa heat shock protein, mitochondrial (Hspd1)
P26772	10 kDa heat shock protein, mitochondrial (Hspe1)
Q56R18	Importin subunit alpha (Kpna3)
Q5U1W8	High-mobility group nucleosome binding domain 1 (LOC100911295)
Q63910	Alpha globin (LOC287167)
Q5M7V3	LOC367586 protein (LOC367586)
D4A5L9	Protein LOC679794 (LOC679794)
D3ZTH8	Protein LOC689899 (LOC689899)
B2RYP6	LUC7-like 2 (S. cerevisiae) (Luc7l2)
Q66HR2	Microtubule-associated protein RP/EB family member 1 (Mapre1)
O35821	Myb-binding protein 1A (Mybbp1a)
Q63357	Unconventional myosin-Id (Myo1d)
B2RYX0	Naca protein (Naca)
G3V6H9	Nucleosome assembly protein 1-like 1 (Nap1l1)
Q56A27	Nuclear cap-binding protein subunit 1 (Ncbp1)
P13383	Nucleolin (Ncl)
P19804	Nucleoside diphosphate kinase B (Nme2)
Q8K1Q0	Glycylpeptide N-tetradecanoyltransferase 1 (Nmt1)
D3ZMY7	Protein Nt5c2 (Nt5c2)
A0A0G2KB27	Protein Nup62cl (Nup62cl)
A0JPJ7	Obg-like ATPase 1 (Ola1)
B2RYG6	Ubiquitin thioesterase OTUB1 (Otub1)
Q6AYD3	Proliferation-associated protein 2G4 (Pa2g4)
O88767	Protein deglycase DJ-1 (Park7)
P06765	Platelet factor 4 (Pf4)
P16446	Phosphatidylinositol transfer protein alpha isoform (Pitpna)
F7EPH4	Protein Sar1a (Ppa1)
Q6DGG0	Peptidyl-prolyl cis-trans isomerase D (Ppid)
P09321	Prolactin-3B1 (Prl3b1)
A0A0G2K0W9	Proteasome subunit alpha type (Psma7)
P40307	Proteasome subunit beta type-2 (Psmb2)
Q4V8E2	Proteasome (Prosome, macropain) 26S subunit, non-ATPase, 14 (Psmd14)
Q5U2S7	Proteasome (Prosome, macropain) 26S subunit, non-ATPase, 3 (Psmd3)
Q3B8P5	Psmd8 protein (Fragment) (Psmd8)
P83868	Prostaglandin E synthase 3 (Ptges3)
Q63011	Zero beta-globin (Fragment) (Q63011)

Table A2. *Cont.*

Accession	Protein Names
P62494	Ras-related protein Rab-11A (Rab11a)
P62828	GTP-binding nuclear protein Ran (Ran)
D4A2G9	Protein Ranbp1 (Ranbp1)
Q71UF4	Histone-binding protein RBBP7 (Rbbp7)
B2RZA9	Ube2l3 protein (rCG_36772)
G3V7V6	All-trans-13,14-dihydroretinol saturase, isoform CRA_b (Retsat)
D4AD70	Protein RGD1561636 (RGD1561636)
P62907	60S ribosomal protein L10a (Rpl10a)
Q4V8I6	60S ribosomal protein L11 (Rpl11)
P23358	60S ribosomal protein L12 (Rpl12)
P24049	60S ribosomal protein L17 (Rpl17)
D3ZPN7	Protein LOC100360604 (Rpl21)
P17077	60S ribosomal protein L9 (Rpl9)
P19945	60S acidic ribosomal protein P0 (Rplp0)
P19944	60S acidic ribosomal protein P1 (Rplp1)
P63326	40S ribosomal protein S10 (Rps10)
D3ZHB3	40S ribosomal protein S12 (Rps12)
A0A0H2UHQ8	40S ribosomal protein S17 (Rps17)
A0A0H2UHT6	40S ribosomal protein S18 (Rps18)
A0A0H2UHG7	40S ribosomal protein S20 (Rps20)
P62850-2	Isoform 2 of 40S ribosomal protein S24 (Rps24)
A0A0H2UHU0	40S ribosomal protein S25 (Rps25)
O55215	Ribosomal protein S2 (Rps2-ps6)
P62083	40S ribosomal protein S7 (Rps7)
Q0D2L6	Protein Rragc (Rragc)
Q6AXV4	Sorting and assembly machinery component 50 homolog (Samm50)
Q6AY18	Protein Sar1a (Sar1a)
Q7TP42	Ab2-292 (Sec62)
Q63556	Serine protease inhibitor A3M (Fragment) (Serpina3m)
G3V7T6	Protein Sf3b1 (Sf3b1)
A0A0G2K8K0	Protein Sfpq (Sfpq)
B5DES0	Protein Snrpd2 (Snrpd2)
M0R907	Protein Snrpd3 (Snrpd3)
P38656	Lupus La protein homolog (Ssb)
O35814	Stress-induced-phosphoprotein 1 (Stip1)
Q6AYB6	Synapse associated protein 1 (Syap1)
Q9EQS0	Transaldolase (Taldo1)
I6L9G6	Protein Tardbp (Tardbp)
P28480	T-complex protein 1 subunit alpha (Tcp1)
P09495	Tropomyosin alpha-4 chain (Tpm4)
P63029	Translationally-controlled tumor protein (Tpt1)
Q498E0	Thioredoxin domain-containing protein 12 (Txndc12)
F2Z3T9	Protein U2af2 (U2af2)
Q9EQX9	Ubiquitin-conjugating enzyme E2 N (Ube2n)
Q9JJP9	Ubiquilin-1 (Ubqln1)
B0BN55	Uroporphyrinogen decarboxylase (Urod)
F1LM09	Ubiquitin carboxyl-terminal hydrolase (Usp7)
G3V8A5	Protein Vps35 (Vps35)
Q80U96	Exportin-1 (Xpo1)
P63102	14-3-3 protein zeta/delta (Ywhaz)
Q8VIL3	ZW10 interactor (Zwint)

References

1. Chan, J.C.; Nugent, B.M.; Bale, T.L. Parental Advisory: Maternal and Paternal Stress Can Impact Offspring Neurodevelopment. *Biol. Psychiatry* **2018**, *83*, 886–894. [CrossRef] [PubMed]
2. Li, Y.J.; Yang, L.P.; Hou, J.L.; Li, X.M.; Chen, L.; Zhu, J.H.; Wang, Q.Y.; Li, G.; Zhao, P.Y.; Liu, X.H.; et al. Prenatal Stress Impairs Postnatal Learning and Memory Development via Disturbance of the cGMP-PKG Pathway and Oxidative Phosphorylation in the Hippocampus of Rats. *Front. Mol. Neurosci.* **2020**, *13*, 158. [CrossRef] [PubMed]

3.	Dahlerup, B.R.; Egsmose, E.L.; Siersma, V.; Mortensen, E.L.; Hedegaard, M.; Knudsen, L.E.; Mathiesen, L. Maternal stress and placental function, a study using questionnaires and biomarkers at birth. *PLoS ONE* **2018**, *13*, e0207184. [CrossRef]

4.	Van den Bergh, B.R.H.; van den Heuvel, M.I.; Lahti, M.; Braeken, M.; de Rooij, S.R.; Entringer, S.; Hoyer, D.; Roseboom, T.; Räikkönen, K.; King, S.; et al. Prenatal developmental origins of behavior and mental health: The influence of maternal stress in pregnancy. *Neurosci. Biobehav. Rev.* **2020**, *117*, 26–64. [CrossRef] [PubMed]

5.	Mathiesen, L.; Bay-Richter, C.; Wegener, G.; Liebenberg, N.; Knudsen, L.E. Maternal stress and placental function; ex vivo placental perfusion studying cortisol, cortisone, tryptophan and serotonin. *PLoS ONE* **2020**, *15*, e0233979. [CrossRef]

6.	Lund, R.J.; Kyläniemi, M.; Pettersson, N.; Kaukonen, R.; Konki, M.; Scheinin, N.M.; Karlsson, L.; Karlsson, H.; Ekholm, E. Placental DNA methylation marks are associated with maternal depressive symptoms during early pregnancy. *Neurobiol. Stress* **2021**, *15*, 100374. [CrossRef]

7.	Wang, Q.; Pan, M.; Zhang, T.; Jiang, Y.; Zhao, P.; Liu, X.; Gao, A.; Yang, L.; Hou, J. Fear Stress During Pregnancy Affects Placental m6A-Modifying Enzyme Expression and Epigenetic Modification Levels. *Front. Genet.* **2022**, *13*, 927615. [CrossRef]

8.	Aushev, V.N.; Li, Q.; Deyssenroth, M.; Zhang, W.; Finik, J.; Hurd, Y.L.; Nomura, Y.; Chen, J. Placental gene network modules are associated with maternal stress during pregnancy and infant temperament. *FASEB J. Off. Publ. Fed. Am. Soc. Exp. Biol.* **2021**, *35*, e21922. [CrossRef]

9.	Francis, J.W.; Hausmann, S.; Ikram, S.; Yin, K.; Mealey-Farr, R.; Flores, N.M.; Trinh, A.T.; Chasan, T.; Thompson, J.; Mazur, P.K.; et al. FAM86A methylation of eEF2 links mRNA translation elongation to tumorigenesis. *Mol. Cell* **2024**, *84*, 1753–1763.e7. [CrossRef]

10.	Yang, S.; Chen, S.; Zhao, Y.; Wu, T.; Wang, Y.; Li, T.; Fu, L.; Ye, T.; Hu, Y.Q.; Chen, H. Identification of a coagulation-related signature correlated with immune infiltration and their prognostic implications in lung adenocarcinoma. *Thorac. Cancer* **2023**, *14*, 3295–3308. [CrossRef]

11.	Petrenko, V.; Vrublevskaya, V.; Bystrova, M.; Masulis, I.; Kopylova, E.; Skarga, Y.; Zhmurina, M.; Morenkov, O. Proliferation, migration, and resistance to oxidative and thermal stresses of HT1080 cells with knocked out genes encoding Hsp90α and Hsp90β. *Biochem. Biophys. Res. Commun.* **2023**, *674*, 62–68. [CrossRef]

12.	Zhang, H.; Zheng, T.; Qin, C.; Zhang, X.; Lin, H.; Huang, X.; Liu, Q.; Chang, S.; Zhang, L.; Guo, J.; et al. CCT6A promotes cell proliferation in colon cancer by targeting BIRC5 associated with p53 status. *Cancer Gene Ther.* **2024**, *31*, 1151–1163. [CrossRef]

13.	Brannigan, R.; Cannon, M.; Tanskanen, A.; Huttunen, M.O.; Leacy, F.P.; Clarke, M.C. The association between subjective maternal stress during pregnancy and offspring clinically diagnosed psychiatric disorders. *Acta Psychiatr. Scand.* **2019**, *139*, 304–310. [CrossRef]

14.	Jensen Pena, C.; Monk, C.; Champagne, F.A. Epigenetic effects of prenatal stress on 11beta-hydroxysteroid dehydrogenase-2 in the placenta and fetal brain. *PLoS ONE* **2012**, *7*, e39791. [CrossRef] [PubMed]

15.	Lévy, F. Neuroendocrine control of maternal behavior in non-human and human mammals. *Ann. D'endocrinologie* **2016**, *77*, 114–125. [CrossRef] [PubMed]

16.	Hellgren, M. Hemostasis during normal pregnancy and puerperium. *Semin. Thromb. Hemost.* **2003**, *29*, 125–130. [CrossRef] [PubMed]

17.	Ciurea, E.L.; Berceanu, C.; Voicu, N.L.; Pirnoiu, D.; Berceanu, S.; Stepan, A.E. Morphological Survey of Placenta in Trombophilia Related Hypoperfusion of Maternal-Fetal Blood Flow. *Curr. Health Sci. J.* **2018**, *44*, 85–91.

18.	Austin, A.W.; Wissmann, T.; von Kanel, R. Stress and hemostasis: An update. *Semin. Thromb. Hemost.* **2013**, *39*, 902–912. [CrossRef]

19.	von Känel, R. Acute mental stress and hemostasis: When physiology becomes vascular harm. *Thromb. Res.* **2015**, *135* (Suppl. 1), S52–S55. [CrossRef]

20.	Simcox, L.E.; Ormesher, L.; Tower, C.; Greer, I.A. Thrombophilia and Pregnancy Complications. *Int. J. Mol. Sci.* **2015**, *16*, 28418–28428. [CrossRef]

21.	Kupferminc, M.J. Thrombophilia and pregnancy. *Reprod. Biol. Endocrinol. RB&E* **2003**, *1*, 111.

22.	Ozmen, A.; Unek, G.; Korgun, E.T. Effect of glucocorticoids on mechanisms of placental angiogenesis. *Placenta* **2017**, *52*, 41–48. [CrossRef] [PubMed]

23.	Drobinskaia, A.N.; Nadeeva, A.P.; Zhukova, V.A.; Pasman, N.M.; Karpov, M.A.; Teliatnikova, N.V. Placental morphology in inherited thrombophilia. *Arkhiv Patol.* **2014**, *76*, 33–36.

24.	Chen, M.; Chao, B.; Xu, J.; Liu, Z.; Tao, Y.; He, J.; Wang, J.; Yang, H.; Luo, X.; Qi, H. CPT1A modulates PI3K/Akt/mTOR pathway to promote preeclampsia. *Placenta* **2023**, *133*, 23–31. [CrossRef]

25.	Liu, Z.; Hong, Z.; Qu, P. Proteomic Analysis of Human Endometrial Tissues Reveals the Roles of PI3K/AKT/mTOR Pathway and Tumor Angiogenesis Molecules in the Pathogenesis of Endometrial Cancer. *BioMed Res. Int.* **2020**, *2020*, 5273969. [CrossRef]

26.	Zhao, H.; Wong, R.J.; Stevenson, D.K. The Impact of Hypoxia in Early Pregnancy on Placental Cells. *Int. J. Mol. Sci.* **2021**, *22*, 9675. [CrossRef]

27.	Beetch, M.; Akhaphong, B.; Wong, A.; Clifton, B.; Jo, S.; Mohan, R.; Abrahante Llorens, J.E.; Alejandro, E.U. Impact of placental mTOR deficiency on peripheral insulin signaling in adult mice offspring. *J. Mol. Endocrinol.* **2023**, *71*, e230035. [CrossRef]

28.	Gupta, M.B.; Jansson, T. Novel roles of mechanistic target of rapamycin signaling in regulating fetal growth†. *Biol. Reprod.* **2019**, *100*, 872–884. [CrossRef] [PubMed]

29. Vaughan, O.R.; Fisher, H.M.; Dionelis, K.N.; Jeffreys, E.C.; Higgins, J.S.; Musial, B.; Sferruzzi-Perri, A.N.; Fowden, A.L. Corticosterone alters materno-fetal glucose partitioning and insulin signalling in pregnant mice. *J. Physiol.* **2015**, *593*, 1307–1321. [CrossRef]

30. Basso, A.D.; Solit, D.B.; Chiosis, G.; Giri, B.; Tsichlis, P.; Rosen, N. Akt forms an intracellular complex with heat shock protein 90 (Hsp90) and Cdc37 and is destabilized by inhibitors of Hsp90 function. *J. Biol. Chem.* **2002**, *277*, 39858–39866. [CrossRef]

31. Liu, Y.; Wang, S.; Ding, D.; Yu, Z.; Sun, W.; Wang, Y. Up-Regulation of Cdc37 Contributes to Schwann Cell Proliferation and Migration After Sciatic Nerve Crush. *Neurochem. Res.* **2018**, *43*, 1182–1190. [CrossRef] [PubMed]

32. Zhu, Y.; Wu, F.; Hu, J.; Xu, Y.; Zhang, J.; Li, Y.; Lin, Y.; Liu, X. LDHA deficiency inhibits trophoblast proliferation via the PI3K/AKT/FOXO1/CyclinD1 signaling pathway in unexplained recurrent spontaneous abortion. *FASEB J. Off. Publ. Fed. Am. Soc. Exp. Biol.* **2023**, *37*, e22744. [CrossRef] [PubMed]

33. Zohn, I.E. Hsp90 and complex birth defects: A plausible mechanism for the interaction of genes and environment. *Neurosci. Lett.* **2020**, *716*, 134680. [CrossRef] [PubMed]

34. Chang, C.; Tang, X.; Woodley, D.T.; Chen, M.; Li, W. The Distinct Assignments for Hsp90α and Hsp90β: More Than Skin Deep. *Cells* **2023**, *12*, 277. [CrossRef]

35. Xinmin, L.; Liping, Y.; Haijiao, W.; Jianghui, Z.; Junlin, H.; Xianghong, Z. Correlation between cognitive development and levels of dopamine and 3, 4-dihydroxyphenylacetic acid in the hippocampus in 80-day-old neonatal rats born of fear-impaired pregnant rats. *Chin. J. Comp. Med.* **2017**, *11*, 10–14.

36. Liping, Y.; Gai, L.; Haijiao, W.; Jianghui, Z.; Xinmin, L.; Junlin, H.; Xianghong, Z. Effects of terror stress of the pregnant rats on emotional changes of 21-day-old neonatal offspring. *CJTCMP* **2018**, *01*, 62–64.

37. Geng, S.; Yang, L.; Cheng, F.; Zhang, Z.; Li, J.; Liu, W.; Li, Y.; Chen, Y.; Bao, Y.; Chen, L.; et al. Gut Microbiota Are Associated with Psychological Stress-Induced Defections in Intestinal and Blood-Brain Barriers. *Front. Microbiol.* **2019**, *10*, 3067. [CrossRef]

38. Takeuchi, T.; Iwanaga, M.; Harada, E. Possible regulatory mechanism of DHA-induced anti-stress reaction in rats. *Brain Res.* **2003**, *964*, 136–143. [CrossRef]

39. Smart, J.L.; Dobbing, J. Vulnerability of developing brain. II. Effects of early nutritional deprivation on reflex ontogeny and development of behaviour in the rat. *Brain Res.* **1971**, *28*, 85–95. [CrossRef]

40. Wu, S.; Gao, Q.; Zhao, P.; Gao, Y.; Xi, Y.; Wang, X.; Liang, Y.; Shi, H.; Ma, Y. Sulforaphane produces antidepressant- and anxiolytic-like effects in adult mice. *Behav. Brain Res.* **2016**, *301*, 55–62. [CrossRef]

41. Wang, T.; Chen, H.; Lv, K.; Ji, G.; Zhang, Y.; Wang, Y.; Li, Y.; Qu, L. iTRAQ-based proteomics analysis of hippocampus in spatial memory deficiency rats induced by simulated microgravity. *J. Proteom.* **2017**, *160*, 64–73. [CrossRef] [PubMed]

42. Szklarczyk, D.; Gable, A.L.; Nastou, K.C.; Lyon, D.; Kirsch, R.; Pyysalo, S.; Doncheva, N.T.; Legeay, M.; Fang, T.; Bork, P.; et al. The STRING database in 2021: Customizable protein-protein networks, and functional characterization of user-uploaded gene/measurement sets. *Nucleic Acids Res.* **2021**, *49*, D605–D612. [CrossRef] [PubMed]

43. Xu, M.; Shi, J.; Min, Z.; Zhu, H.; Sun, W. A Network Pharmacology Approach to Uncover the Molecular Mechanisms of Herbal Formula Kang-Bai-Ling for Treatment of Vitiligo. *Evid. Based Complement. Alternat. Med.* **2019**, *2019*, 3053458. [CrossRef] [PubMed]

44. Liu, H.; Lü, Z.; Tian, C.; Ouyang, W.; Xiong, Y.; You, Y.; Chen, L.; Deng, Y.; Zhao, X.; Sun, X. Mechanism of Shenbing decoction III in the treatment of proteinuria in chronic kidney disease: A network pharmacology-based study. *Nan Fang Yi Ke Da Xue Xue Bao* **2019**, *39*, 227–234.

45. Bindea, G.; Mlecnik, B.; Hackl, H.; Charoentong, P.; Tosolini, M.; Kirilovsky, A.; Fridman, W.H.; Pagès, F.; Trajanoski, Z.; Galon, J. ClueGO: A Cytoscape plug-in to decipher functionally grouped gene ontology and pathway annotation networks. *Bioinformatics* **2009**, *25*, 1091–1093. [CrossRef]